Theses and Dissertations

Summer 2014

Examining the feasibility of magnetic source MRI by studying fMRI acquisition and analysis strategies

Leo Ai
University of Iowa

Recommended Citation

Ai, Leo. "Examining the feasibility of magnetic source MRI by studying fMRI acquisition and analysis strategies." PhD (Doctor of Philosophy) thesis, University of Iowa, 2014.
http://ir.uiowa.edu/etd/1284.

EXAMINING THE FEASIBILITY OF MAGNETIC SOURCE MRI BY STUDYING

FMRI ACQUISITION AND ANALYSIS STRATEGIES

by

Leo Ai

A thesis submitted in partial fulfillment
of the requirements for the Doctor of
Philosophy degree in Biomedical Engineering
in the Graduate College of
The University of Iowa

August 2014

Thesis Supervisor: Associate Professor Jinhu Xiong

Graduate College
The University of Iowa
Iowa City, Iowa

CERTIFICATE OF APPROVAL

_____

PH.D. THESIS

_____

This is to certify that the Ph.D. thesis of

Leo Ai

has been approved by the Examining Committee
for the thesis requirement for the Doctor of Philosophy
degree in Biomedical Engineering at the August 2014 graduation.

Thesis Committee: _____
                        Jinhu Xiong, Thesis Supervisor

                    _____
                        Edwin L. Dove

                    _____
                        Vincent A. Magnotta

                    _____
                        Joseph M. Reinhardt

                    _____
                        Daniel R. Thedens

ACKNOWLEDGEMENTS

ABSTRACT

Magnetic source magnetic resonance imaging (msMRI) is an fMRI technique that has been under development for direct detection of neuronal magnetic fields to map brain activity and has been shown to be experimentally detectable using conventional means, but there is debate on the detection of the msMRI signal since it can be only a 0.2% change. Detection of its temporal characteristics has yet to be reported and may strengthen the case for msMRI detection. The temporal characteristics of the detected msMRI signal were examined in this work, but it was found that the sensitivity of conventional analysis techniques are low within the context of msMRI, preventing consistent msMRI signal detection and analysis of its temporal characteristics. Examination of blood oxygen level dependent (BOLD) contrast contamination and application of mean-shift clustering (MSC) to fMRI analysis were performed to look into the possibility of improving the low sensitivity. fMRI analysis is commonly performed with cross correlation analysis (CCA) and techniques based on the General Linear Model (GLM), but both CCA and GLM techniques typically perform calculations on a per-voxel basis and do not consider relationships neighboring voxels may have. MSC is a technique to consider for this purpose and shows improved activation detection for both simulated and real BOLD fMRI data. To consider the issue of BOLD contamination, the hemodynamic response over time was examined using repeated median nerve stimulation. On average, the results show the BOLD signal is not detectable after the second fMRI run. The results are consistent with previous hemodynamic habituation effect studies with other types of stimulation, but they do not completely agree with

findings of evoked potential studies. Overall, this work shows that the low detection sensitivity may be able to be addressed with the purpose of furthering msMRI research.

TABLE OF CONTENTS

LIST OF TABLES

LIST OF FIGURES

CHAPTER I

INTRODUCTION

Blood oxygen level dependent (BOLD) functional magnetic resonance imaging (fMRI) is an imaging technique introduced in the early 1990s and is currently commonly used to study brain function (Belliveau et al. 1991, Bandettini et al. 1992, Kwong et al. 1992, Ogawa et al. 1992). The BOLD fMRI technique, like all current fMRI techniques, relies on measuring regional cerebral hemodynamics to infer neuronal activity, but may not accurately represent neuronal activity due to the indirect nature of the technique. Also, regional cerebral hemodynamics used to infer neuronal activity changes on the order of seconds, where neuronal activity happens on the order of milliseconds. The temporal resolution of such fMRI techniques are therefore unable to measure brain activity that happens on such time scale due to the relatively poor temporal resolution inherent to the technique.

Magnetic source MRI (msMRI) is an fMRI technique that has been under development with the intent of directly assessing neuronal function. The technique is based on directly detecting MRI signal changes using changes in magnetic fields caused by firing neurons, which would address the issues of temporal resolution and the issues of accurately representing neuronal activity in theory. There are mathematical models that show the msMRI signal is detectable (Blagoev et al. 2007, Cassara et al. 2008, Konn et al. 2003, Pell et al. 2006, Xue et al. 2006) and studies that show experimental detection is possible (Bianciardi et al. 2004, Bodurka et al. 1999, Bodurka et al. 2002, Chow et al. 2006a, Chow et al. 2006b, Liston et al. 2004, Petridou et al. 2006, Scott et al. 1992, Song et

al. 2001, Truong et al. 2006, Xiong et al. 2003, Xue et al. 2009), but temporal characteristics of the msMRI signal has not yet been reported. However, it was found that the sensitivity of conventional analysis techniques are too low within the context of msMRI to consistently detect the msMRI signal, which is likely further exacerbated by the fact that experimental data has shown that the msMRI signal can be only about a 0.2% change (Xue et al. 2009) as well as other issues such as BOLD contamination. To address the issue of detection sensitivity, studies in cerebral hemodynamics (BOLD habituation in particular) and application of mean-shift clustering (MSC) in fMRI analysis were performed to examine possible methods of increasing detection sensitivity.

Examinations in cerebral hemodynamics may give insight into when BOLD habituation may affect the BOLD signal. If there are scenarios when the BOLD signal is reduced or cannot be detected, it may indicate a scenario where BOLD contamination (a commonly brought up issue in msMRI research) could be minimized. If such a situation can be replicated within the context of msMRI and potentially further minimize BOLD contamination, it may strengthen the case for msMRI signal detection. Adopting MSC into fMRI analysis was attempted to examine the possibility of improving detection sensitivity from an analysis standpoint. Currently used analysis techniques typically perform calculations on a per voxel basis, meaning any relationships voxels may have with each other are not taken into consideration. MSC is a clustering technique based on density calculations on a feature space of chosen image characteristics, which addresses the issues of taking into consideration neighboring characteristics. If the incorporation of MSC in fMRI analysis can improve detection sensitivity in low signal to noise (SNR) situations as seen in msMRI, it may be possible to improve msMRI signal detection as

well. The results from these studies show that there is some promise of improving msMRI detection sensitivity.

CHAPTER II

BACKGROUND

Magnetic Resonance Imaging

Magnetic Resonance Imaging (MRI) is a medical imaging technique commonly used to image the body for medical diagnosis and research purposes. MRI is based on the quantum property of spin (a fundamental property of protons, neutrons, and electrons) which can be seen in atoms with unpaired protons or neutrons. This means that such atoms can be used to generate magnetic resonance images in theory. When such atoms are placed in a magnetic field (B_0), they will absorb energy at a very specific frequency (Larmour frequency) as well as align in the same direction (parallel) or in the opposite direction (anti-parallel) of the B_0 field. Despite there being only slightly more parallel spins (5 parts per million at 1.5 Tesla for example), it is this difference that provides a net magnetic moment along the direction of the B_0 field and the source of the MRI signal.

The atoms can be excited with a radio frequency pulse (B_1) at the Larmour frequency for the desired atom. The B_1 field tips the spins to a specific flip angle so it is no longer aligned with B_0, causing the spins to precess around the B_0 direction. Magnetic gradients are applied to selectively alter the B_0 field, causing spins to precess at different frequencies at specific locations. By using a B_1 pulse in the shape of a sinc function, the gradients allows the targeted excitation of spins that are in a specific spatial range because the spins would have a specific range of frequencies that would be matched by the applied B_1 pulse. As the spins precess after being excited, a signal known as the free

induction decay is produced and used to reconstruct the image by using the inverse Fourier transform.

The aforementioned precession of spins does not happen indefinitely as they will eventually return to their equilibrium state in the B_0 field. The process where the z component of the net magnetization, the component parallel to B_0, relaxes or returns the equilibrium state is called T_1 relaxation. The T_1 time constant describes the rate at which the z component of magnetization recovers. It is mostly affected by the environment or "lattice" in which the magnetization resides, which is why T_1 relaxation is also commonly referred to as spin-lattice relaxation. Likewise, the magnetization on the x-y plane, the component perpendicular to B_0, will eventually decay to zero to return to the equilibrium state. This process is called T_2 relaxation where the T_2 time constant describes the rate at which the x-y magnetization component decays. The T_2 time constant depends only on interactions between neighboring spins in an ideal situation, thus T_2 relaxation is also called spin-spin relaxation. In real systems, differences in chemical environments as well as inhomogeneities in the magnetic field exist, which in practice creates a shorter time constant referred to as T_2^*.

Different tissues have different T_1, T_2, and T_2^* relaxation times, which can be detected in the MRI signal to produce different contrast images. There are also other mechanisms that can affect the relaxation times to produce more different types of contrast images, such as the BOLD contrast used in fMRI.

BOLD fMRI Technique

BOLD fMRI was introduced in the early 1990s and is used to detect neuronal activity (Bandettini et al. 1992, Belliveau et al. 1991, Kwong et al. 1992, Ogawa et al. 1990). The BOLD technique utilizes the detection of changes in blood flow and blood oxygenation in the brain. Since neurons do not store energy internally, oxygenated blood must constantly be delivered to the brain in the form of oxyhemoglobin. When the oxygen is delivered and used, the oxyhemoglobin becomes deoxyhemoglobin. Due to the oxygen molecule that is not present, deoxyhemoglobin is paramagnetic, while oxyhemoglobin is diamagnetic. This change in magnetic properties of the hemoglobin can be observed as a change in T_2* relaxation. An increase in T_2* in an area of the brain would indicate a higher concentration of oxyhemoglobin and a higher BOLD signal intensity while higher concentrations of deoxyhemoglobin would lower BOLD signal intensity. The concentration of these different types of hemoglobin in specific regions of the brain change based on the metabolic demands of the neurons, making it possible to infer neuronal activity. While other fMRI techniques exist, Arterial Spin Labeling for example, the BOLD technique is currently the most commonly used. However, all current fMRI techniques depend on measuring regional cerebral hemodynamics to infer neuronal activity in one form or another.

BOLD fMRI Technique Shortcomings

The BOLD fMRI technique depends on measuring regional cerebral hemodynamics which has drawbacks by nature since using regional cerebral hemodynamic measurements means that neuronal activity is not directly detected, but

inferred. The detected signal may not necessarily reflect neuronal activity as the relationship between regional cerebral hemodynamics and the underlying neuronal activity is often non-linear and complex (Fox 1986). Regional cerebral hemodynamics can also be affected by other sources (drug effects for example) without change in the underlying neuronal activity. With BOLD contrast, the signal also tends to be vascular in nature since larger BOLD signals may be detected in areas with larger and/or more veins (Lai et al. 1993). There is also the issue of temporal resolution of current fMRI techniques, which is on the order of seconds since cerebral hemodynamics itself responds in that time frame. This is slow when compared to neuronal firings, which occurs on the order of milliseconds, meaning fMRI techniques based on regional cerebral hemodynamics cannot detect neuronal signals that require a high temporal resolution. While there are methods of addressing these shortcomings using other functional imaging techniques, there is currently no single technique that can address all of the aforementioned issues with current fMRI techniques while providing the same benefits of fMRI, high spatial resolution for example. Techniques can be combined to address individual shortcomings (Schulz et al. 2004), but doing so increases cost and complexity of the technique as well as not necessarily addressing inherent shortcomings of the individual techniques.

Development of msMRI

The msMRI technique is currently under development with the intent of addressing the shortcomings of current functional imaging techniques. The technique is designed to directly detect neuronal activity by using an MRI to examine neuronal

magnetic fields generated during neuron firings. Directly detecting magnetic fields generated by neuron firings should in principle address the issues of low temporal resolution and accurate representation of brain activity associated with fMRI techniques based on cerebral hemodynamics. Neuronal activity generates ionic current along dendrites and axons which generates a weak transient magnetic field around the neuron, changing the precession rate of nuclear spins. Spins exposed to the neuronal magnetic field will lose phase coherence, causing a decrease in MRI signal strength. It is well established that this change in magnetic field is detectable at the scalp with MEG (Cohen 1968). Theoretical models of msMRI also indicate that the change in magnetic field can cause a signal change which is detectable with the MRI (Blagoev et al. 2007, Cassara et al. 2008, Konn et al. 2003, Pell et al. 2006, Xue et al. 2006,).

To model the magnetic fields generated by neuronal activity, each dendrite and axon is modeled as a current dipole to model the magnetic fields generated by neuronal activity. The magnetic field can be calculated at any point around a neuron using the Biot-Savart law. Since the majority of axons in the brain are myelinated, neuronal current of axons are concentrated at the nodes of Ranvier in the form of through-membrane current. It has been experimentally demonstrated that this type of current generates a negligible net magnetic field and can be safely ignored (Swinney and Wikson, 1980). The magnetic field generated by the dendrites can thus be considered the main source of the neuronal magnetic field. The orientation of dendrites relative to each other also needs to be considered since orientation can have an effect on the net neuronal magnetic field. If dendrites are organized in a parallel configuration, there would be a net magnetic field generated. If the dendrites are organized in an anti-parallel orientation, the individual

magnetic fields generated would add destructively, resulting in no net magnetic field. In the best case scenario, it has been calculated that the msMRI signal changes could be up to 2% (Xue et al. 2006).

Issues of msMRI

Despite having been shown to be experimentally detectable, there are concerns that have caused msMRI signal detection to be questioned. The detected signal can only about a 0.2% change despite the theoretical model suggesting that the signal can be upwards of a 2% change, making it difficult to determine if the detected activation is the msMRI signal in actuality. Another issue commonly brought up in msMRI signal detection is BOLD contamination, which is when a BOLD signal still exists in the image and potentially masks the msMRI signal. Xue et al. (2009) managed this issue by using a stimulation paradigm designed purposely to force the BOLD signal to reach a constant state with the msMRI signal superimposed on top of the BOLD signal and detected, thus minimizing the issue of BOLD contamination. However, BOLD contamination is an issue still generally not considered to be fully addressed.

Temporal Characteristics of msMRI

Since msMRI activation detection is still considered to be debatable, examinations on strengthening its detection is required to further this field of study. One method of doing so is to examine the temporal characteristics of the detected msMRI signal which has not yet been reported. The msMRI signal has previously been reported to be detectable using electrical median nerve stimulation (Xue et al. 2009), and temporal

characteristics of this stimulation type has been well studied (Allison et al. 1989a, Allison et al. 1989b), making it a reasonable choice for continued use in msMRI research.

The known electrical waveform in the brain due to electrical median nerve stimulation can be used in the examination of the temporal characteristics of the msMRI signal. Since mathematical models have shown that the msMRI signal is dependent on the neuronal magnetic field, it stands to reason that the theoretical msMRI response function can be calculated provided the neuronal response function is known. The aforementioned electrical waveform due to median nerve stimulation can be considered to be analogous with the neuronal response function, which then can be used to calculate the theoretical waveform and compared with the measured waveform. If both the theoretical and measured waveform share specific temporal characteristics, it may strengthen the case for msMRI signal detection. However, it was found that detection sensitivity using conventional techniques was low and the msMRI signal and its temporal characteristics could not be reliably detected. To address the issue of low detection sensitivity, studies were performed with the intent of improving detection sensitivity of msMRI by examining the use of mean-shift clustering in fMRI analysis and examining the issue of BOLD contamination, both of which may prove beneficial to msMRI studies as well as fMRI studies in general.

Mean Shift Clustering

Mean-shift clustering (MSC) was examined for use in fMRI analysis in general with possible application to msMRI and fMRI analysis. Techniques based on cross-correlation analysis (CCA) and the General Linear Model (GLM) are commonly used for

fMRI data analysis (Bandettini et al. 1993, Boynton et al. 1996, Bullmore et al. 1996, Calhoun et al. 2001, Cohen et al. 1997, Friston et al. 2004, Penny et al. 2003), however these techniques are not without drawbacks. Both techniques typically perform their calculations on a per voxel basis. This means that each calculation does not take into consideration any relationship that neighboring voxels may have with each other. This has the effect of lowering the sensitivity of the technique when attempting to identify activations, which is especially true in low contrast to noise ratio (CNR) situations.

There has been interest in enhancing fMRI data analysis using cluster size tests with various techniques having been examined with that intention. Cluster analysis (based on random field theory) is commonly used to help isolate activations (Foreman et al. 1995, Worsley et al. 1992, Xiong et al. 1995). K-means clustering (MacQueen 1967) is a method where observations are partitioned into "k" number of clusters where each observation belongs to the cluster with the closest mean. Fuzzy clustering (Bezdek et al. 1984) is similar to k-means clustering, except that fuzzy clustering takes into consideration that a single observation can belong to more than one cluster. Both K-means and Fuzzy clustering have been examined for improving fMRI data analysis (Baumgartner et al. 1997, Baumgartner et al. 1998, Moser et al. 1997, Singh et al. 1996). Mean-shift clustering (MSC) is another technique to consider for the same purpose.

The MSC technique was first introduced by Fukunaga et al. (1975) for examining pattern recognition, but the technique was mostly unexplored until more recently (Cheng 1995, Dorin et al. 2002). The technique has found uses in image processing and vision tasks. Image segmentation has also been explored with this technique on brain images (Mayer et al. 2009). MSC revolves around a density estimation that is done on a

predetermined feature space. Intuitively, the technique works by calculating the mean shift vector, then shifting the kernel as dictated by the mean shift vector. This process is repeated as appropriate until convergence at which time a cluster in the feature space can be identified. By selectively choosing the features used for the feature space, it would be possible to incorporate characteristics of the data that normally would not be part of the analysis with CCA and GLM based techniques. MSC also offers some other advantages with regards to implementation. The technique does not require assumptions to be made about noise distribution. Compared to typical cluster analysis, no hard cut-off in cluster size is required with MSC. Since MSC is based on density estimation of a feature space, it does not make any assumption on the shape of the clusters either as well as allowing different feature spaces to be used to incorporate different characteristics of the data into analysis. These advantages with MSC may allow higher sensitivity when detecting activations for improved results.

BOLD Habituation

To examine the issue of BOLD contamination in msMRI signal detection, a closer examination of how cerebral hemodynamics behaves over time with identically repeated stimulation was performed. This phenomenon examined is also referred to as habituation, which is defined as a decrease in an elicit behavior resulting from the repeated presentation of an eliciting stimulus. Habituation has been of interest to many researchers and has been studied using fMRI for different brain systems and with various types of stimuli (Becerra et al. 1999, Dirnberger et al. 2004, Fischer et al. 2000, Pfeiderer et al. 2002, Mosbascher et al. 2010, Seitz et al. 1992, Talavage et al. 1999, Taylor et al. 1978,

Tomberg et al. 1989). Habituation from repeated presentation of visual stimulations is characterized by a decrease of activity in the primary visual region and can occur in brief sessions (Fischer et al. 2000). Significant habituation has also been found in the primary auditory cortex with repeated presented auditory stimuli (Pfeiderer et al. 2002, Talavage et al. 1999). Pain stimuli have been used in similar studies which have found the habituation effect to be present (Becerra et al. 1999, Mosbascher et al. 2010). Research involving motor stimulations has shown that the detected signal does decrease over time (Dirnberger et al. 2004, Seitz et al. 1992, Taylor et al. 1978). Critically, these studies demonstrate that cerebral hemodynamic signals should typically habituate over time when repeatedly presented with the same stimuli.

In tandem with the habituation studies of cerebral hemodynamic signals, habituation of evoked potential signals of the human brain has been also widely studied (Allison et al. 1989a, Allison et al. 1989b, Thees et al. 2003). In particular, several research groups have carefully studied the habituation effects of electrical stimulation of the median nerve (Ozkul et al. 2002, Restuccia et al. 2011). It was reported by Thees et al. (2003) that the overall signal strength of brain response in the motor and sensorimotor areas does not significantly change over a one-hour recording period, suggesting that the overall signal strength is not sensitive to habituation. However, there are also studies that have shown that habituation does affect particular peaks of the response waveform despite the overall signal strength being relatively constant (Ozkul et al. 2002, Restuccia et al. 2011). Such studies have shown that the N20 peak is susceptible to habituation effects. Ozkul et al. (2002) reported a significant decrease in the N20 peak (14.4 ± 4.70%) over a period of four hundred stimulations among healthy volunteers. A similar

study performed by Restuccia et al. (2011) also reported a significant decrease in the amplitude of the N20 peak after three thousand stimulations. Unlike cerebral hemodynamic signals which typically habituate over various types of stimuli, evoked potential habituation is apparently more complex. The overall signal strength in the S1 region does not appear to be affected significantly by habituation (Thees et al. 2003), but the same may not be true for specific peaks (N20 for example) in the waveform (Ozkul et al. 2002, Restuccia et al. 2011).

Cerebral hemodynamic responses with median nerve stimulation have also been reported (Arthurs et al. 2004, Backes et al. 2000, Ferretti et al. 2003, Feretti et al. 2007). These studies all utilized median nerve stimulation over a period of time and did show changes in the recorded Blood Oxygen Level Dependent (BOLD) signal in their results, but it should be noted that none of the studies had a specific focus on the habituation effect. The study performed by Arthurs et al. (2004) focused on how attention may affect the measured BOLD signal. Ferretti et al. (2003, 2007) focused on how pain delivered with median nerve stimulation can affect the measured BOLD signal. Since these studies did not have habituation as the main focus, the stimulations delivered typically varied over time in some way (e.g., intensity, frequency). To investigate the habituation effects, the stimuli delivered would ideally be identically repeated throughout the duration of the study. Backes et al. (2000) performed a study that utilized identically repeated stimuli, but the volunteers were asked to perform attention tasks (counting total number of interruptions in stimulations) during the study. It is possible that the measured BOLD signal reflects the task effects rather than possible habituation effects in such scenarios. Habituation has been studied using other forms of stimuli as previously mentioned, but

cerebral hemodynamic habituation of median nerve stimulation has not yet been reported to the best of our knowledge.

Electrical stimulation of the median nerve has been commonly used in the clinical setting to identify the somatosensory and motor cortex with intra-operative direct cortical recordings (Allison et al. 1989a, Allison et al. 1989b). Direct cortical recordings are considered to be the gold standard in measuring evoked potentials because it provides spatially and temporally accurate information. The BOLD fMRI technique (Kwong et al. 1992, Ogawa et al. 1990) measures cerebral hemodynamic changes induced by neuronal activity of the brain. Combining direct cortical recordings with the BOLD technique offers a good opportunity to study the coupling between evoked potentials and cerebral hemodynamics (Heeger et al. 2000, Logothetis et al. 2001) as well as the behavior of coupling over repeated stimulations. As the first step, the presented study investigated the hemodynamic habituation effects of the median nerve stimulation using fMRI. Follow-ups to this study would involve directly comparing cerebral hemodynamics (BOLD) with evoked potentials. A better understanding of BOLD habituation may be able to mitigate the issue of BOLD contamination and improve sensitivity in msMRI signal detection considering BOLD contamination is a commonly brought up issue in msMRI research because the msMRI signal itself is small and may be masked by unwanted BOLD signals.

Relationship of MSC and BOLD Habituation to msMRI

The examination of low detection sensitivity by studying BOLD habituation and application of MSC into fMRI analysis may further develop the field of msMRI research. Examining habituation with identical repeated median nerve stimulation would allow a

better understanding of how regional cerebral hemodynamics correlates with the underlying neuronal activity which may give more insight on when the BOLD contamination is an issue while investigating msMRI signal detection. If there are scenarios with no BOLD signals detected, it may give strength to msMRI signal detection if such situations can be similarly replicated, further minimizing BOLD contamination. The examination of MSC adoption into fMRI analysis investigated how it may improve the sensitivity of fMRI analysis in general with application in msMRI analysis. The MSC technique allows the consideration of different image characteristics which are normally not part of CCA or GLM based fMRI analysis techniques, which may improve activation detection in general by maintaining low false positive rates in low CNR situations. Also considering that the MSC technique by itself does not require a hard kernel size threshold, it may also improve highly focused activation detection. Since msMRI activations could be considered to be highly focused activations and occur in low CNR situations, msMRI detection may receive benefits from these aspects of the proposed MSC technique. Further examination of these two topics may help in the development of msMRI activation detection.

CHAPTER III

THEORY AND METHODS

fMRI Data Acquisition – msMRI Temporal Characteristics

Twelve subjects (6 females, 6 males, ages 20-44) gave informed written consent with the approval of the University of Iowa's Institutional Review Board. All subjects reported that they were right-handed, not using medications at the time of scanning, healthy, and had no history of any mental or psychiatric conditions. All ten subjects were scanned at the University of Iowa's Medical Education and Research Facility.

The msMRI data was acquired on a Siemens 3T Trio scanner (Siemens Medical Solutions, Erlangen, Germany) using a gradient echo EPI pulse sequence with the following MRI parameters: TR = 100ms, TE = 30ms, flip angle = 21º, matrix = 64 x 64, FOV = 220mm, slice thickness = 5mm with 20% gap, 180 images per run, 4000 images per scan. Three runs were performed per scanning session. BOLD fMRI data was acquired on the same MRI machine using a gradient echo EPI pulse sequence with the following MRI parameters: TR = 2000ms, flip angle = 90 degrees, TE = 30ms, matrix = 64 x 64, FOV = 220mm, slice thickness = 5mm with 20% gap, 180 images per run. Only one run was performed per scanning session. A T1 anatomical scan was also performed with the following parameters: TR = 1590ms, flip angle = 10 degrees, TE = 3.39ms, matrix = 128 x 128, FOV = 220mm, slice thickness = 2mm.

Unilateral electrical stimulation was delivered to the subject's right median nerve using a Grass S48 stimulator (Grass Technologies, West Warwick, Rhode Island, USA). The delivered stimulations were square wave pulses with 0.2ms duration between 70-

120V, enough to obtain a thumb twitch. For the msMRI scans, a randomized inter-stimulation interval (ISI) between 200-300 ms was used for the duration of each run. The BOLD scan used a block design of four and a half off/on cycles (40 seconds off, 40 seconds on) with an ISI of 600 ms. A randomized ISI was used to reduce any effect that expecting a stimulation occurring with a fixed inter stimulation interval might have on the resulting BOLD signal. The volunteers were asked to passively feel the stimulation, stay still, stay awake, and not actively perform anything else for the duration of the scan.

fMRI Data Acquisition – MSC and Habituation

Ten subjects (5 females, 5 males, age 22-32) gave informed written consent with the approval of the University of Iowa's Institutional Review Board. All subjects reported that they were right-handed, not using medications at the time of scanning, healthy, and had no history of any mental or psychiatric conditions. All ten subjects were scanned at the University of Iowa's Medical Education and Research Facility

BOLD fMRI data was acquired on a Siemens 3T Trio scanner (Siemens Medical Solutions, Erlangen, Germany) using a gradient echo EPI pulse sequence with the following MRI parameters: TR = 2000ms, flip angle = 90 degrees, TE = 30ms, matrix = 64 x 64, FOV = 220mm, slice thickness = 5mm with 20% gap, 180 images per run. Each run was six minutes in length. Each scanning session was composed of seven of runs, though only the first run was used for the purposes of the MSC study. A T1 anatomical scan was also performed with the following parameters: TR = 1590ms, flip angle = 10 degrees, TE = 3.39ms, matrix = 128 x 128, FOV = 220mm, slice thickness = 2mm.

Unilateral electrical stimulation was delivered to the subject's right median nerve using a Grass S48 stimulator (Grass Technologies, West Warwick, Rhode Island, USA). The stimulation voltage used was 15 volts above the motor threshold, which was individually defined as the minimum voltage required to obtain a thumb twitch. The delivered stimulations were square wave pulses with 0.2ms duration. A block design of four and a half off/on cycles (40 seconds off, 40 seconds on) with a randomized inter-stimulation interval (ISI) between 1.0-2.0 seconds was used. A randomized ISI was used to reduce any effect that expecting a stimulation occurring with a fixed inter stimulation interval might have on the resulting BOLD signal. The volunteers were asked to passively feel the stimulation, stay still, stay awake, and not actively perform anything else for the duration of the scan.

Simulated Data – MSC

The simulated data was designed to emulate fMRI data using one hundred images, 128x128 matrix size, and with a block design of two and a half off/on cycles (20 images per off or on cycle). Activations of various sizes (20x20, 10x10, 2x2 voxels) were inserted onto the data for analysis. Gaussian noise at different CNRs (0.20, 0.40, 0.06, and 0.80) was generated and inserted into the simulated data.

Time Locked Averaging – Temporal Characteristics of msMRI

The examination of msMRI temporal characteristics requires the use of time locked averaging with a randomly sampled waveform. By using a randomly generated ISI for the stimulation paradigm, the neuronal response function in the MRI effectively

becomes randomly sampled. Locking time to stimulation onset allows calculating the time locked averages for the measured msMRI waveform, which making a comparison between it and the theoretical msMRI waveform possible. The theoretical msMRI waveform as detected by the MRI scanner needs to be calculated based on the neuronal response function using median nerve stimulation for comparison with the measured waveform. It has been shown from mathematical models that the msMRI signal is dependent on the neuronal magnetic field originating from dendrites of the neurons. The magnetic field generated by a single dendrite can be calculated with the Biot-Savart Law:

$$\vec{B}_d(x,y,z,t) = \frac{\mu_o}{4\pi} \int \frac{i d\vec{l} \times \vec{r}}{r^3}$$
[1]

The overall neuronal magnetic field $\vec{B}$ is the sum of multiple $\vec{B}_d$ from each dendrite:

$$\vec{B}(x,y,z,t) = \sum \vec{B}_d(x,y,z,t)$$
[2]

The waveform of $\vec{B}$ can be detected by measuring evoked potentials with direct recording from an exposed cortical brain surface and can be used to determine the NRF. The component of $\vec{B}$ parallel to $\vec{B}_o$ field of scanner causes spins to acquire additional phase, which can be described as:

$$\phi(x,y,z,t) = \int_{t-TE/2}^{t+TE/2} \gamma B_{//}(x,y,z,t_1)\cos(\theta)dt_1$$
[3]

where ϕ is acquired phase, TE is the echo time during MRI acquisition, γ is the

gyromagnetic ratio, $\vec{B}_{//}$ is the component of $\vec{B}$ parallel to $\vec{B}_o$, and θ is the angle

between $\vec{B}$ and $\vec{B}_o$. The MRI signal for an image voxel can then be shown as:

$$S(t) = \int_0^{\Delta x} \int_0^{\Delta y} \int_0^{\Delta z} \rho(x, y, z) e^{i\phi(x,y,z,t)} dx dy dz \qquad [4]$$

where S(t) is the MRI signal for the voxel, ϕ is still acquired phase, and ρ is spin

density within the voxel. Using the neuronal response function using median nerve

stimulation with direct recordings from an exposed cortical brain surface as reported by

Allison et al. (1989) (Figure 1), the waveform of MRI signal, $S(t)$, can be theoretically

calculated using Eq. 2-4 (Figure 2), which would then be used for comparison purposes

with the measured msMRI waveform.

MSC Theory

The proposed MSC technique was evaluated using both simulated and real fMRI

data. The data analysis was performed using Cross Correlation Analysis (CCA) to

generate a statistical parametric image (SPI). The mean-shift clustering was then applied

to a feature space constructed using selected characteristics of the SPI. Comparisons were

made among CCA, CCA plus cluster analysis (CCA+CA), and CCA + MSC to examine

the application of MSC.

MSC is based on density estimation of a predetermined multi-modal feature space

of image characteristics. Previously used feature spaces, such as perceived color

(Connolly 1996, Wyszecki et al. 1982), are generally not applicable to fMRI analysis

since color is not a feature that would be of interest. For this study, a feature space of the estimated Z values of the SPI and the mean voxel values surrounding a voxel in the same SPI (eight neighboring voxels in 2D and twenty six neighboring voxels in 3D) was used as they can be features of interest and incorporating them in the analysis may help with activation detection. The estimated Z values were used because it relates directly to statistical significance, and the mean voxel value of the surrounding voxels were used to take into consideration neighboring effects. The image features are mapped into a point in a multi-dimension space. The density is calculated within a defined kernel on the feature space. The kernel is moved based on the density gradient in the feature space until the local maximum is found. Points in the feature space associated with the same local maximum are considered to belong to the same cluster, and the calculation is repeated until all points are assigned to a cluster.

Using the Parzen window technique (Parzen 1962), the kernel density estimation at point x can be described by:

$$\hat{f}(x) = \frac{c_k}{nh^d} \sum_{i=1}^{n} k\left(\left\| \frac{x - x_i}{h} \right\|^2 \right)$$ [5]

where n is the number of data points, c_k is a constant, k is the kernel, h is the kernel size, and d is the number of dimensions in the feature space. The local maximum density is identified at $\nabla \hat{f}(x) = 0$ by moving the kernel based on the gradient ascent in the feature space. Equation 5 can be rewritten as:

$$\nabla \hat{f} = \frac{2c_k}{nh^{d+2}} \sum_{i=1}^{n} (x - x_i) k' \left(\left\| \frac{x - x_i}{h} \right\|^2 \right)$$

[6]

Assuming g(x) = -k'(x), the gradient density estimator can then be described as:

$$\nabla \hat{f} = \frac{2c_k}{nh^{d+2}} \sum_{i=1}^{n} (x_i - x) g \left(\left\| \frac{x - x_i}{h} \right\|^2 \right)$$

[7]

$$\nabla \hat{f} = \frac{2c_k}{nh^{d+2}} \left[\sum_{i=1}^{n} g \left(\left\| \frac{x - x_i}{h} \right\|^2 \right) \right] \left[\frac{\sum_{i=1}^{n} x_i g \left(\left\| \frac{x - x_i}{h} \right\|^2 \right)}{\sum_{i=1}^{n} g \left(\left\| \frac{x - x_i}{h} \right\|^2 \right)} - x \right]$$

[8]

The first term of Equation 8 is proportional to the density estimate computed with the kernel. The second term:

$$m(x) = \left[\frac{\sum_{i=1}^{n} x_i g \left(\left\| \frac{x - x_i}{h} \right\|^2 \right)}{\sum_{i=1}^{n} g \left(\left\| \frac{x - x_i}{h} \right\|^2 \right)} - x \right]$$

[9]

is the mean shift vector where g is the kernel, h is the kernel size, x is the mean estimate inside the kernel, and x_i is the element inside the kernel. The mean shift vector, m(x), defines how the kernel will move along the density gradient towards the local maximum which corresponds with dense regions in the feature space. This calculation is performed at each data point, shifted by m(x) along the density gradient, and repeated until convergence is reached when local maximum is found. This procedure allows the mean

shift clustering technique to identify such locations without having to estimate the probability density function of the associated data. Points associated with the same local maximum belong to the same cluster.

Within the mean-shift vector equation, the parameter that likely has the largest effect on the analysis is the kernel size, h, as differences in kernel sizes can change the density estimates calculated which the MSC technique is based on. While adaptive techniques do exist, a range of kernel sizes was used to examine how the technique behaves.

Temporal Characteristics Analysis

The MRI images were processed using MATLAB (MathWorks Inc., Natick, MA) using custom written software and Analysis of Functional NeuroImages (AFNI) (Cox 1996). The first 200 images were discarded to allow hemodynamics to reach a steady state. A two dimensional motion correction was used. A spatial Gaussian filter with full width half maximum (FWHM) of 3mm was used, and a high pass temporal filter with cutoff frequency 2Hz was applied to remove physiological noise such as heartbeat and respiration. Cross correlation analysis was performed with a statistical z threshold of 3 with a cluster size threshold of 5 voxels were applied to isolate significant activation(s). The reference function used for CCA was based on the calculated theoretical neuronal response function and the known randomized ISIs. The resulting time course was then used as the reference function for the analysis.

For comparison purposes, a time course was extracted for a region of interest from the recorded data. Time locked averages with time locked to stimulation onset, was

performed to generate the measured neuronal response function. A temporal Gaussian filter was applied with a FWHM of 20ms to produce the final measured waveform.

Habituation Data Analysis

The MRI images were processed using AFNI. Three-dimensional motion correction was performed to minimize motion effects. All images were normalized to Talairach space (www.bic.mni.mcgill.ca). Constant, linear, and quadratic trends were identified and removed. A Gaussian filter with full width half maximum of 4mm was used to smooth the images. A reference function was generated by using the hemodynamic response function convolved with the task function. Cross correlation analysis was performed to generate a statistic map using the generated reference function. The Fisher transform was used to convert correlation values to Z statistical values. A statistical threshold of $Z = 3$ (p = 0.0013, uncorrected) and a cluster size threshold of 240 mm³ was used to isolate areas of activations. These Z statistic maps were averaged together with their ten corresponding maps across subjects to produce an average statistic map per corresponding run in the scanning sequence.

MSC Data Analysis

The general approach to the proposed MSC analysis method is applying MSC to a feature space constructed using selected characteristics of the SPI generated using CCA. CCA was chosen over GLM because (1) which technique used to generate the SPI is less important for the purposes of this study; (2) the CCA technique allows easy control over the significance level while it is more difficult to do so with GLM.

The real fMRI images were processed using AFNI and custom Matlab software. As part of the CCA analysis, three-dimensional motion correction was performed to minimize motion effects. All images were normalized to Talairach space. Constant, linear, and quadratic trends were removed. To investigate the effect of a Gaussian filter on activation detection with MSC, no Gaussian filter and a Gaussian filter with full width half maximum (FWHM) of 4mm was applied. SPIs were generated for individual subjects.

MSC Comparisons

The proposed method (CCA+MSC) was compared with typical CCA and CCA plus cluster analysis (CCA+CA) procedure using the same simulated data. Activations of sizes 20x20, 10x10, and 2x2 were inserted onto the data to identify how the techniques behave with different sized activations. The total area of all test patterns was maintained to be the same by varying the number of inserted activations. The 2x2 activation size can be considered to be a simulation for highly focused activations. One thousand different Gaussian white noise patterns were generated and inserted and averaged into the simulated data at per CNR (0.20, 0.40, 0.60, 0.80) for examination on how the technique reacts to noise. No additional smoothing filter was applied to the simulated data.

The proposed technique was assessed based on sensitivity and specificity and compared with the performances of the aforementioned techniques (CCA, CCA+CA, CCA+MSC) on simulated data. True positive rate comparisons were used to examine how the different kernel sizes affected the outcomes at various CNRs, and false positive rate comparisons were used to examine the amount of noise that appear in the results of

each technique. Since simulated data was used, the ground truth is known, so identifying true and false positive rates is a simple task by comparing detected activations with true activations. Receiver operating characteristic (ROC) curves were drawn to allow a direct comparison of performance between the techniques.

The real fMRI data from ten subjects was analyzed for evaluating CCA, CCA+CA, and CCA+MSC. The three techniques are evaluated using both individual fMRI data and averaged fMRI data while controlling significance level at $p = 0.01$. Different statistical thresholds were determined and applied in order to set the significance level to $p = 0.01$ for comparison purposes. The threshold for CCA was calculated to be $z = 4.8$ for the filtered and $z = 4.9$ for the unfiltered (Bonferroni corrected). The CCA+CA used a threshold of $z = 2.6$ which was calculated based on a study performed by Xiong et al. (1995) with a cluster of threshold of 6 voxels for FWHM = 4mm and 4 voxels for the unfiltered dataset. The CCA+MSC used a threshold of $z = 2$ for both filtered and unfiltered data. The z threshold for CCA+MSC was selected based on the results of simulations to achieve an approximate significance level of $p = 0.01$ (see results section).
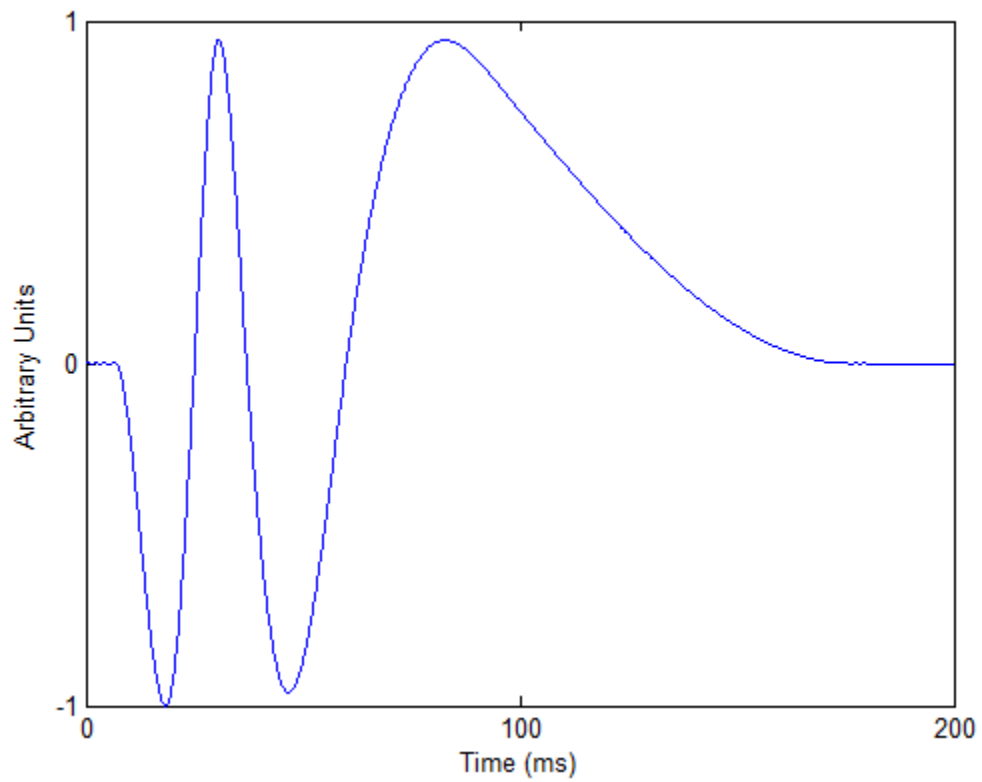
Figure 1: Representation of the reported neuronal response function from measured evoked potentials using direct recordings from an exposed cortical brain surface (Allison et al. 1989)
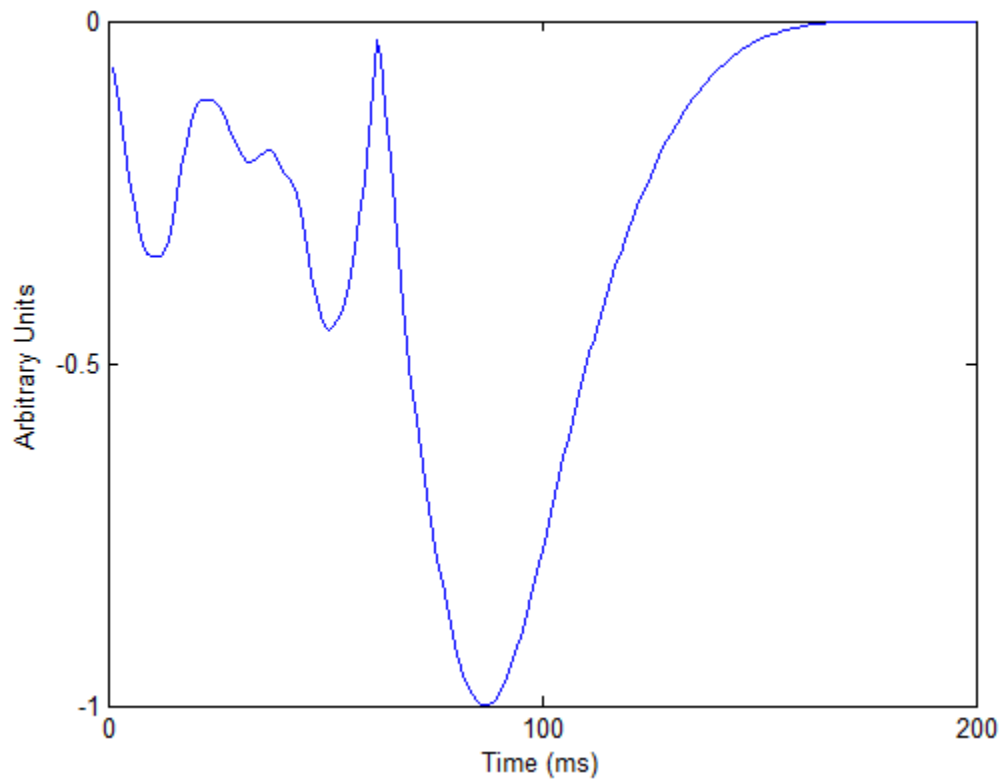
Figure 2: The theoretical neuronal response waveform calculated using Eq. 2-4 based on

the reported neuronal response function (Figure 1). This calculated waveform should be

seen by the MRI scanner in theory and will be compared with the measured waveform.

CHAPTER IV

RESULTS

Temporal Characteristics Results

The msMRI activation map shows activation in the primary motor cortex (M1), which agrees with the BOLD M1 activation (Figure 3). The measured msMRI waveform appears to show similarities in temporal characteristics with the theoretical neuronal response function (Figure 4). Both waveforms have local maximums at similar temporal locations at approximately 0ms and 60ms. Both waveforms also show the largest negative peak at approximately 100ms. While the theoretical neuronal response function approaches zero after approximately 160ms, the measured waveform shows that it does not. This discrepancy may be due to our assumption that the NRF approaches zero after approximately 170ms. It was also found that the M1 activation was not consistently detected across all subjects. Only five of the twelve subjects showed activations in general, indicating that is an issue with detection sensitivity.

Habituation results

Inter-run habituation is shown in figure 5. The data was averaged across all ten subjects. The very first run showed significant activations in the left S1/M1 region of the brain with a statistical threshold of $Z = 3$ ($p = 0.0013$, uncorrected) and with a cluster size threshold of 240 mm³. No significant activations were observed in the remaining six runs.

Figure 6 shows the individual average across runs of activation cluster volume that were found in the left M1/S1 area. Activations were isolated with a statistical

threshold of Z = 3 and a cluster size threshold of 240 mm³. On average, the volume of activation clusters in the first scan is 6253.6 ± 5006.8 mm³. The second scan is 3988.8 ± 3473.7 mm³. The third scan has activations of 2621.6 ± 2762.7 mm³. The fourth scan has activations of 2602.4 ± 2768.5 mm³. The data shows a consistent rapid decrease in the cluster volumes of statistical significance (ANOVA, F = 2.59, p<0.05). It should be noted that run 6 appears to show an unusually high average volume when compared to runs 5 and 7. In the data, one subject showed an unusually large activation in run 6. This can explain why there is a sudden spike in the average; however, an ANOVA test shows that this sudden spike is not statistically significant when compared to runs 5 and 7 (F = 0.56, p>0.05).

Figure 7 shows the average percent change found in individual 3x3x3 voxel regions of interest in the left S1/M1 area of identified activations. A rapid decay in the average percent change can be seen. The first scan has an average percent change of 0.79%. The second scan has an average of 0.48%. The third scan's average was 0.30%. The fourth scan's average was 0.40%. This decay of average percent change is consistent with what is seen in figure 6 (decay in activation voxel size). ANOVA analysis showed that this decrease in percent change is statistically significant (F = 3.10, p<0.05).

Figure 8 shows split-half analysis that was used to show intra-run habituation with average data across all ten subjects. The left image is processed with the first 2.5 cycles of the first run and shows significant activation in the M1/S1 regions on the left side of the brain. The right image is processed with the last 2.5 cycles of the first run and also shows that the activations have been detected in the M1/S1 region on the left side of the brain. The activation size of the right image is smaller than the activation size in the left

image. As before, a statistical threshold of Z = 3 and a volume threshold of 240 mm³ was used.

The average volume of activation clusters from individual half-runs found in M1/S1 from the split-half analysis is shown in Figure 9. A statistical threshold of Z = 3 and volume threshold of 240 mm³ was used. In the first 2.5 cycles, the average volume of activation clusters was 11807.2 ± 4439.7 mm³. The last 2.5 cycles had an average of 8533.6 ± 5284.9 mm³. Paired T-test shows that the volume of the first half is statistically larger than the volume of the second half (t = 2.22, p < 0.05).

<u>MSC results</u>

True Positive Rate Comparison

Using the proposed CCA + MSC technique, true positive rates were plotted to examine the behavior of the technique at various kernel sizes. The statistical threshold was applied at Z = 3. The kernel sizes used were in the range of 0.05 to 0.50. The CNRs of the simulated data are 0.20, 0.40, 0.60, and 0.80. The results show the true positive rate is dependent on the kernel size (Figure 10). Essentially nothing was detected at CNR of 0.20, but the true positive rates can start to decline significantly at a kernel size of 0.20 for CNR = 0.40. For very high CNR (0.80), the true positive rate remains high across the range of kernel sizes used. The true positive rates do fluctuate as the kernel size is changed, but this is expected as the noise is being randomly generated and changing the kernel size likely has an effect on the cluster assignment of the voxels. Figure 10 indicates that the kernel size can be optimized for enhanced activation detection. A kernel

size of 0.20 was used for the rest of the comparisons, although not exclusively, as it seems to be an appropriate choice for most CNR and activation sizes.

False Positive Rate Comparison

False positive rates of the proposed CCA+MSC technique were examined while varying the z threshold (0.1 to 5.0) using simulated data. The same CNRs were used. A kernel size of 0.20 was selected based on the true positive rate comparisons (Figure 10). The false positive rate shows significant improvements over CCA at all simulated activation sizes (Figure 11) despite the curves being similar in shape to the CCA curve. It increases as z threshold decreases until z = 1 where it increases beyond the figure cap of false positive rate 0.05 and thus not shown. The 2x2 case follows the CCA curve more closely than the 10x10 and the 20x20 cases, but an improvement was still seen. The comparison was also made without an activation map (only Gaussian noise), and the result is similar to the 20x20 and 10x10 cases. Figure 12 shows representative activation maps generated by CCA and CCA+MSC with a z = 1 threshold at CNR = 0.80 with a 0.20 kernel size. It can be visually observed that there are less false activations in the case with CCA+MSC, which agrees with the results from Figure 11.

ROC Comparison of Different Kernel Sizes

A comparison was made with ROC curves between CCA, CCA+CA, and the proposed CCA+MSC at the same CNRs as before, and on the same simulated data set (Figure 13). Simulated data was used for this comparison with the statistical threshold varied from Z = 0.1 to 5.0 and the kernel size being set at 0.10, 0.20, and 0.50. The ROC

curves indicate that a properly chosen kernel size, in this case 0.20, show an improvement over CCA and shows similar performance with CCA+CA at certain false positive rates and CNRs. If the kernel size (e.g., 0.50) used is too large, essentially no activations are detected using CCA+MSC at low CNR (0.20), but can show significant improvement over CCA and CCA+CA at higher CNRs (0.40, 0.60, 0.80) with the exception of the 2x2 simulation where CNR of 0.40 also lacked detection. If the kernel size (e.g., 0.10) is too small, the CCA+MSC technique is generally inferior to CCA+CA and performs similarly with CCA.

The relative performance of CCA+MSC and CCA+CA shows a rather complex relationship. In the 20x20 and 10x10 cases at kernel size = 0.20, CCA+CA is better than CCA+MSC at all false positive rates, but can show similar results roughly starting at false positive rate of 0.04. However, CCA+MSC does not show similar results with CCA+CA at CNR 0.20 despite showing improvement over CCA. In the 2x2 case, CCA+MSC appears to be better than CCA+CA up to a false positive rate of about 0.015 with the two techniques performing similarly after that. Significant improvements over CCA+CA can be seen with CCA+MSC at CNRs of 0.60, 0.80, and sometimes 0.40 with kernel size = 0.50, occurring mostly between false positive rates at about 0.0025 to 0.01. Considering that significance level of $p = 0.05$ is commonly used for activation detection, CCA+MSC should show improvement over CCA and sometimes CCA+CA at lower significant levels in a practical situation.

CCA vs CCA+MSC vs CCA+CA on Real Data

The real fMRI data was analyzed using CCA, CCA+CA, and CCA+MSC (Figure 14). Activations are expected to be seen on the left M1/S1 region due to the right median nerve stimulation. The CCA+MSC was applied with different kernel sizes of 0.05, 0.10, 0.15, and 0.20. Based on Figure 11, a threshold of z = 2 was applied to achieve a significance of p=0.01. As shown in Figure 14, the expected activations can be detected using CCA+CA and CCA+MSC with or without a filter in the expected areas while no activation can be seen with standard CCA. Table 1 summarizes the activation volume and average z-scores of the averaged data of both filtered and unfiltered fMRI data. The kernel sizes where activations can be detected for real fMRI is 0.05 and 0.10, which is smaller than the kernel size of 0.20 for the simulated data. Both kernel sizes of 0.05 and 0.10 cases show activations with the 0.10 case showing slightly smaller activations than CCA+CA and the 0.05 case showing larger activations when compared to CCA+CA. In the cases with no filter applied, the detected activations are smaller than their filtered counterparts (Table 1) likely due to the filter enhancing CNR of the SPI, but the non-filtered results generally show the same trends as the filtered results. Individual results are summarized in Table 2 and essentially follow the same trends seen in Table 1. The results show that CCA, CCA+CA, and CCA+MSC (kernel size = 0.10) are statistically different when unfiltered (ANOVA, F = 15.4, p<0.05) or filtered (ANOVA, F = 10.9, p<0.05). The Tukey test further reveals that CCA+MSC is significantly better than CCA in both filtered and unfiltered cases (p = 0.05). The performance of CCA+MSC is statistically similar with CCA+CA (p = 0.05).

The z threshold was also held at z = 2 for comparison purposes between the techniques despite this meaning that the effective p values would differ for each comparison (Figure 15). The expected activations are seen in the expected regions of M1/S1 using all of the mentioned techniques. CCA and CCA+MSC produce similar results where CCA and CCA+MSC shows 139 and 127 activated voxels respectively if unfiltered, 318 and 311 activated voxels respectively if filtered. The CCA+CA results are also similar at 135 voxels if unfiltered and 312 voxels if filtered. It is expected that CCA+CA and CCA+MSC show smaller activation sizes as they are both second steps added to the analysis for removing false positives.
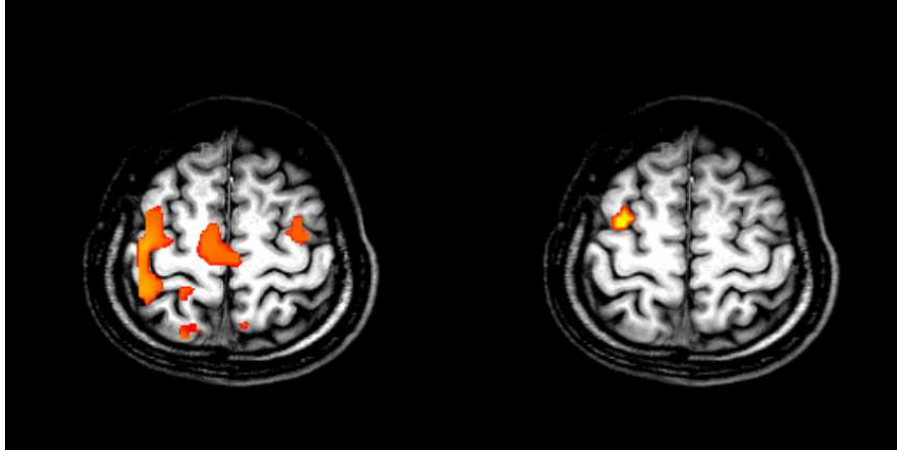
Figure 3: Activations seen due to electrical right median nerve stimulation using BOLD fMRI and msMRI. BOLD (left) activations can be seen in the left M1, S1, and SMA. msMRI (right) activation can be seen in the left M1.
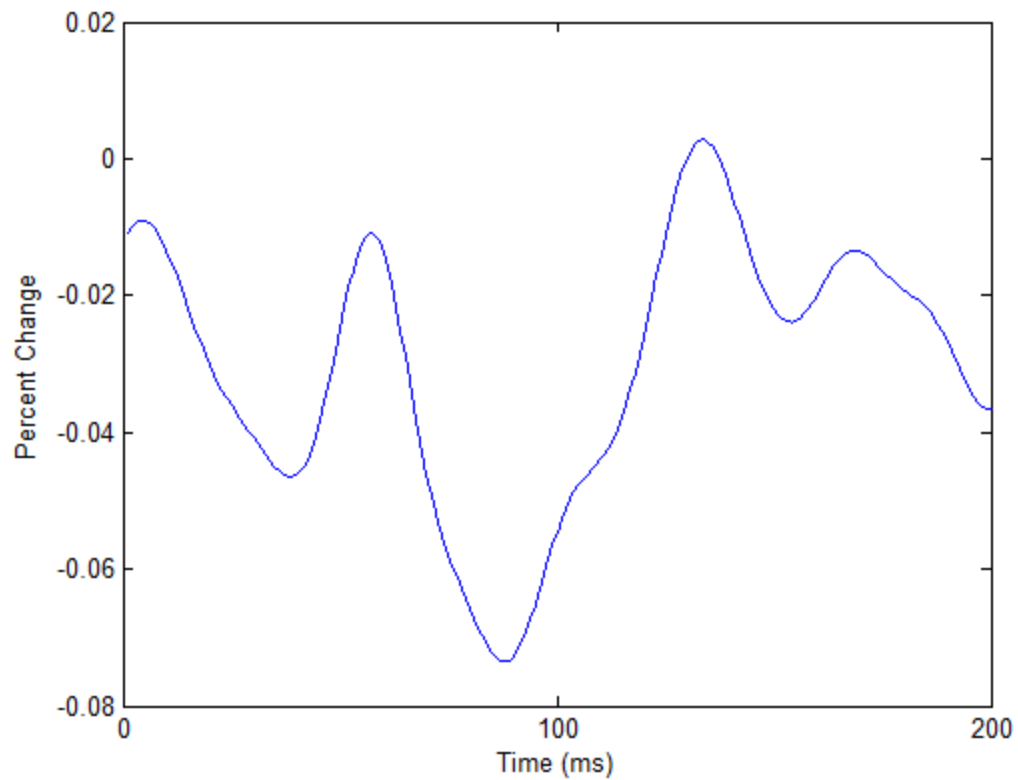
Figure 4: Measured neuronal response function of the left M1 area. The time course was extracted from the left M1 activation seen in the msMRI image and had time locked averaging applied, resulting in the measured neuronal response function.
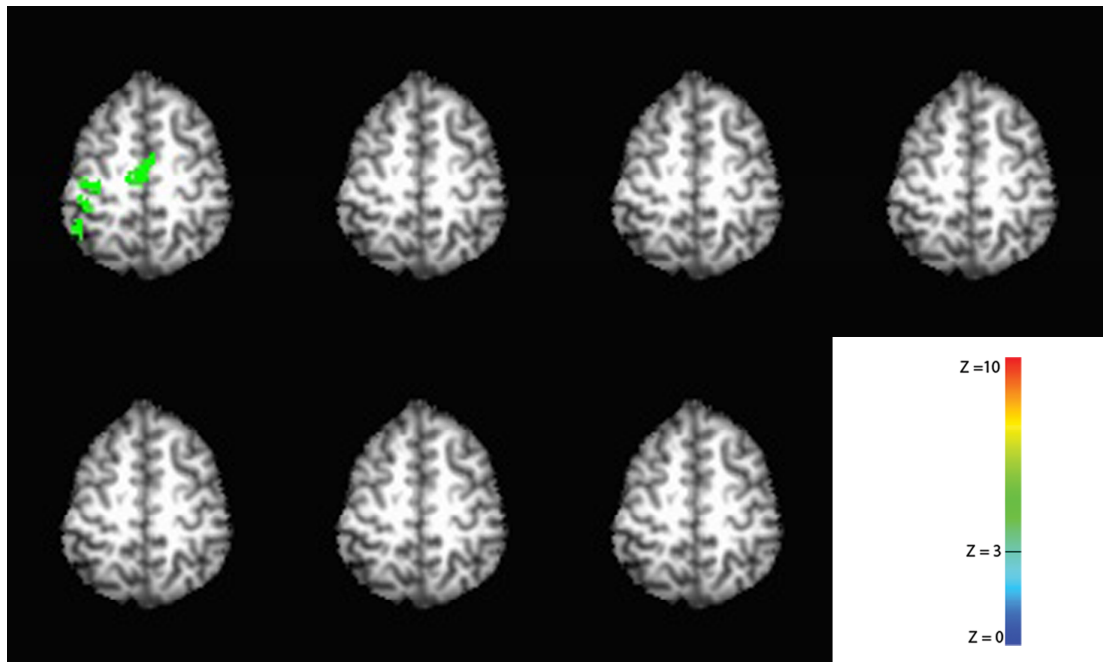
Figure 5: Inter-run habituation effect with median nerve stimulation. Only the very first run showed significant activation. Data was averaged across all ten subjects. A statistical threshold of Z = 3 (p = 0.0013, uncorrected) and a cluster size threshold of 240 mm³ was used to isolate activations. The right hemisphere is on the right and the left hemisphere is on the left.
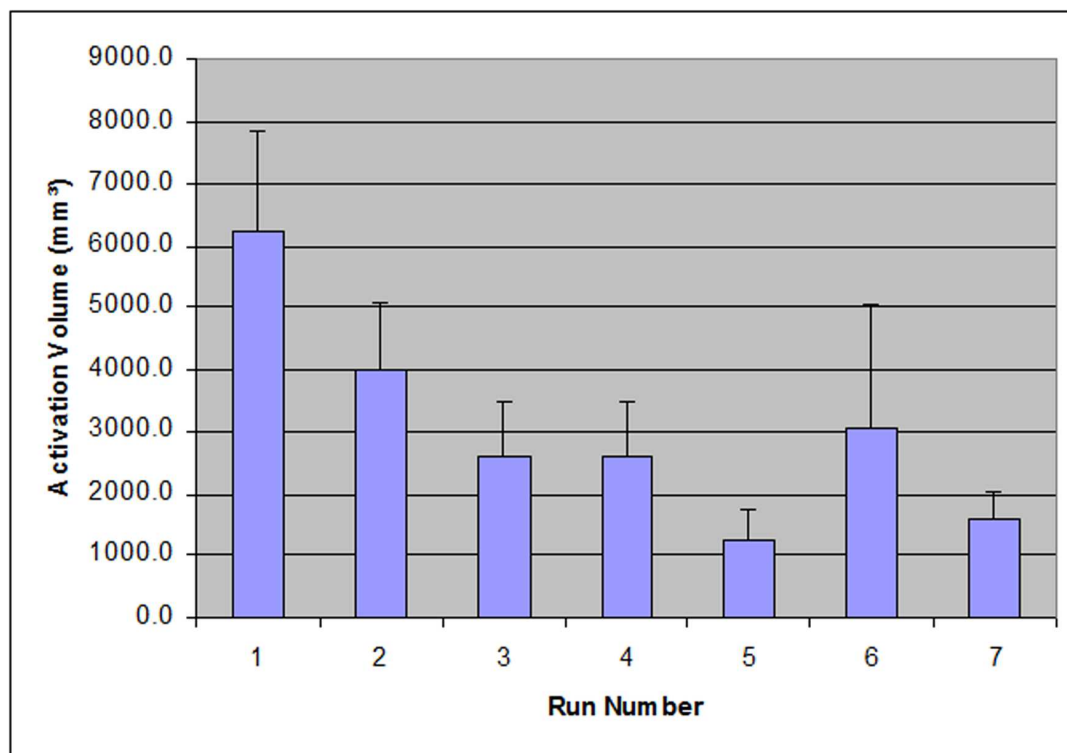
Figure 6: The average volume of activation for seven runs of data acquisition. The activation volumes were measured in the left M1/S1 area. The activation map was generated using a statistical threshold of $Z = 3$ and a volume threshold of 240 mm³. The individual activation volumes across all subjects were identified and averaged. The error bars represent one standard error.
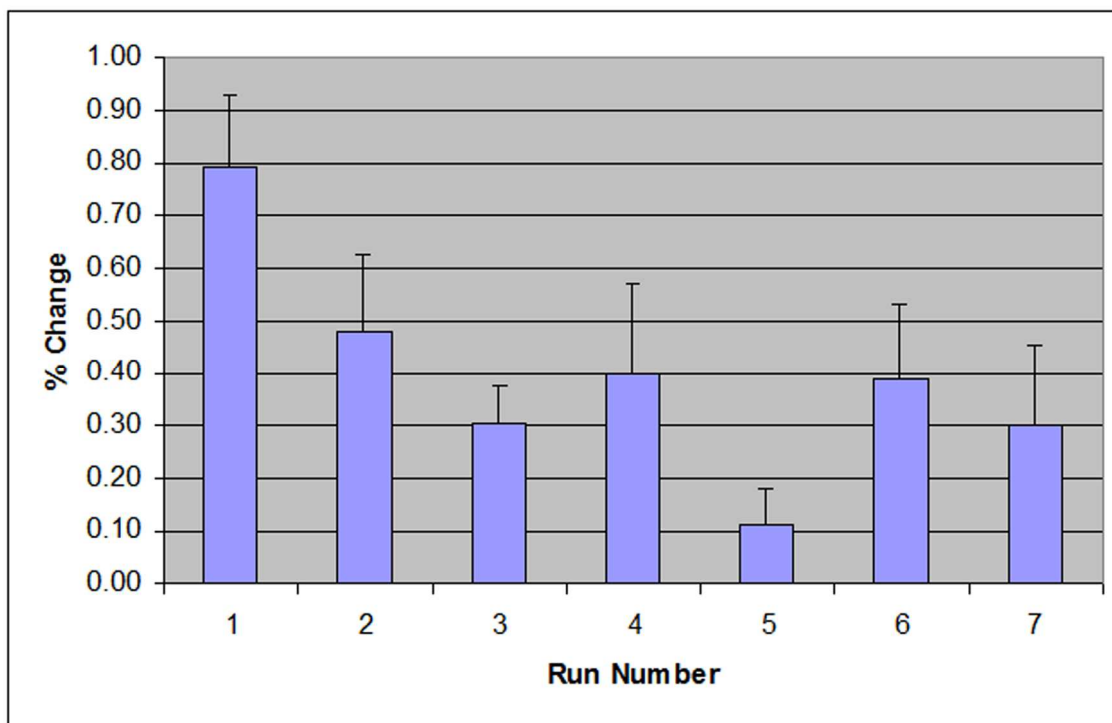
Figure 7: The average percent change in a 3x3x3 voxel region of interest in the S1/M1

area across 7 runs of all subjects. The error bars represent one standard error.
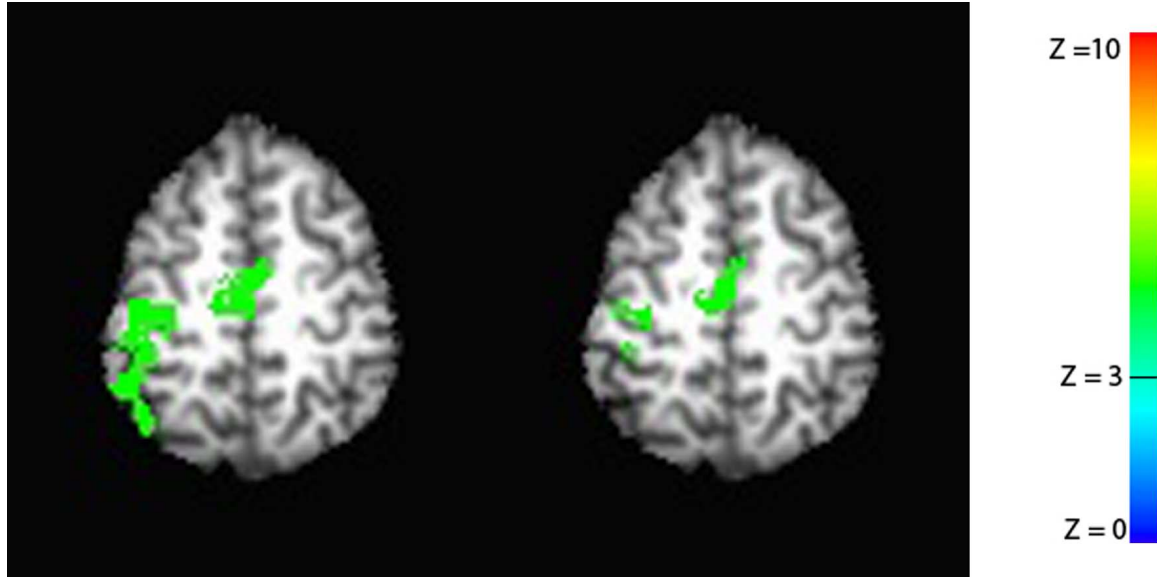
Figure 8: Split-half analysis was used to show intra-run habituation. Only the first run was used. The left image represents activation map processed with the first 2.5 cycle data of the first run. The right image is activation map processed with the last 2.5 cycle data of the first run. A statistical threshold of $Z = 3$ and a volume threshold of 240 mm³ was used. The right hemisphere is on the right and the left hemisphere is on the left.
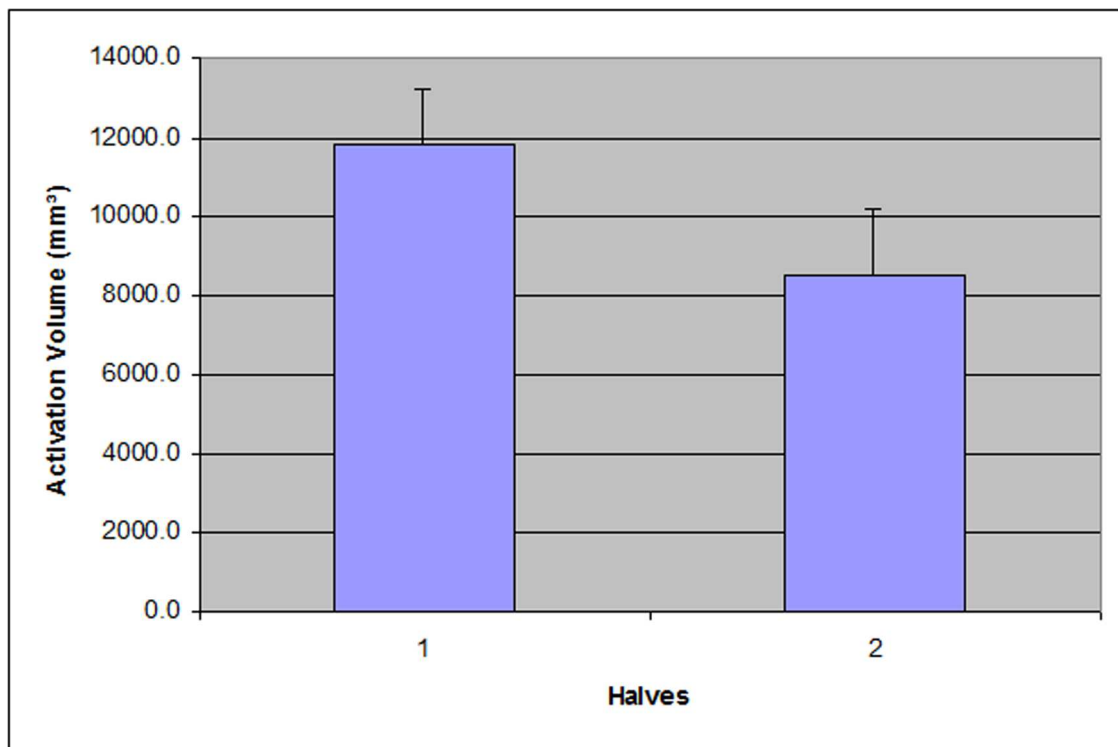
Figure 9: The average volume of activation clusters found in the first and last 2.5 cycles of scan 1 (figure 4). The activation volumes were measured in the left M1/S1 area. The error bars represent one standard error.
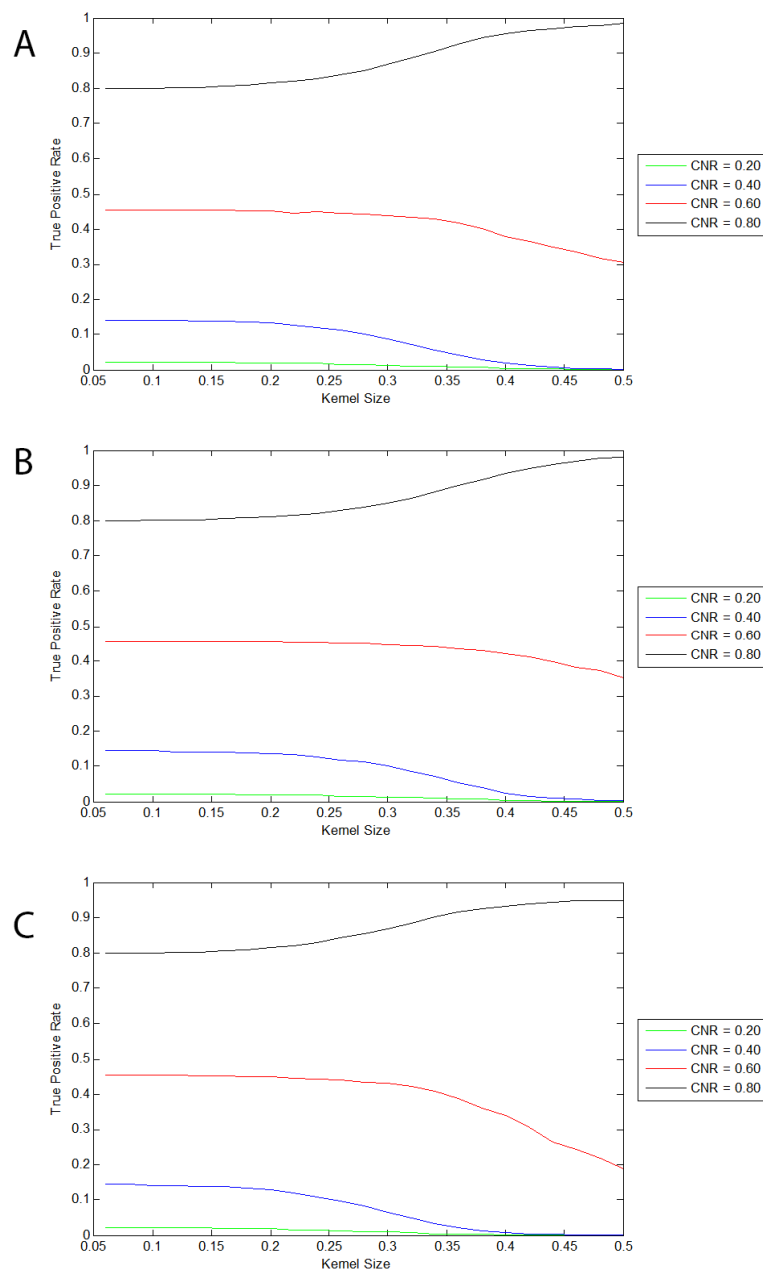
Figure 10: Effect of kernel size on true positive rates for various activation sizes with simulated data. The statistical threshold was held constant at z = 3. A range of kernel sizes was used from 0.05 to 0.50. CNRs used are 0.20, 0.40, 0.60, and 0.80. **A:** 20x20 activation size. B**:** 10x10 activation size. **C:** 2x2 activation size.
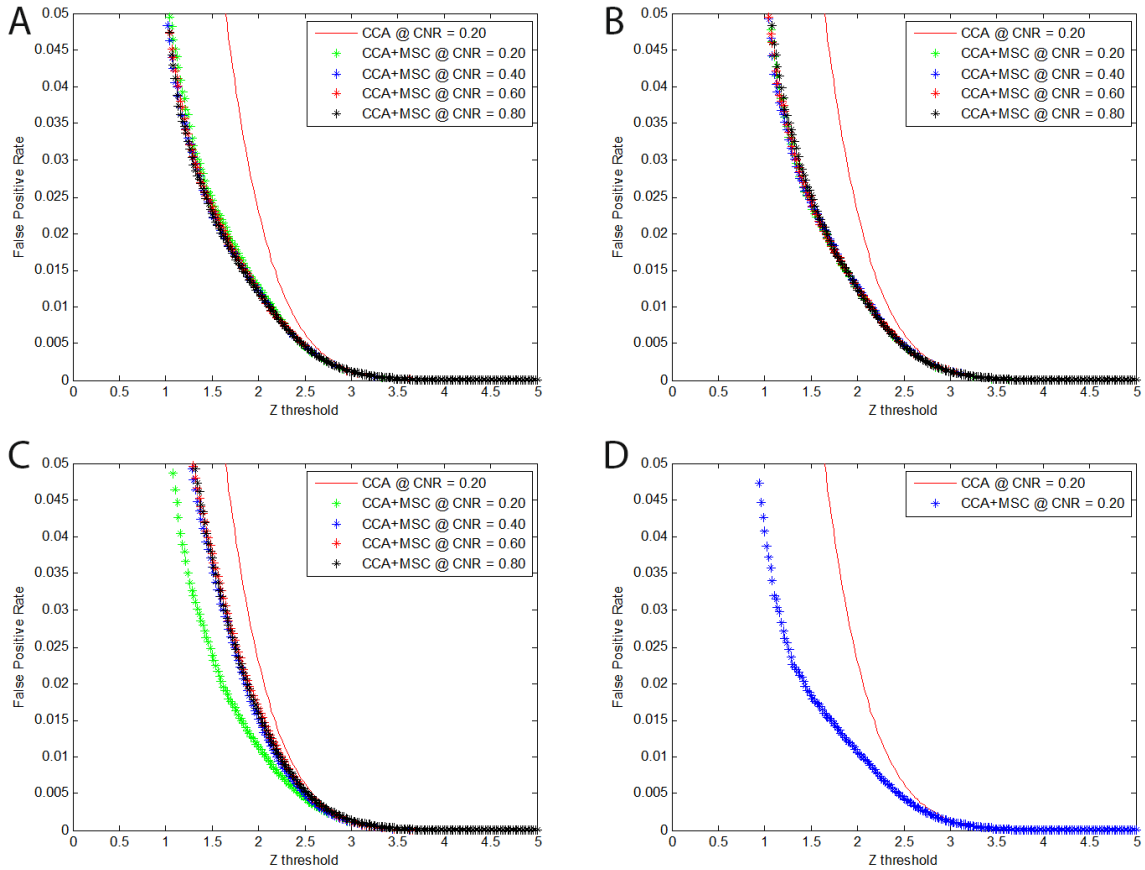
Figure 11: Change of false positive rates at different z thresholds using various activation sizes with simulated data. Kernel size was held constant at 0.20. The z thresholds were varied from 0 to 5. CNRs used are 0.20, 0.40, 0.60, and 0.80. **A:** 20x20 activation size. B**:** 10x10 activation size. **C:** 2x2 activation size. **D:** Activation map consisting of noise only.
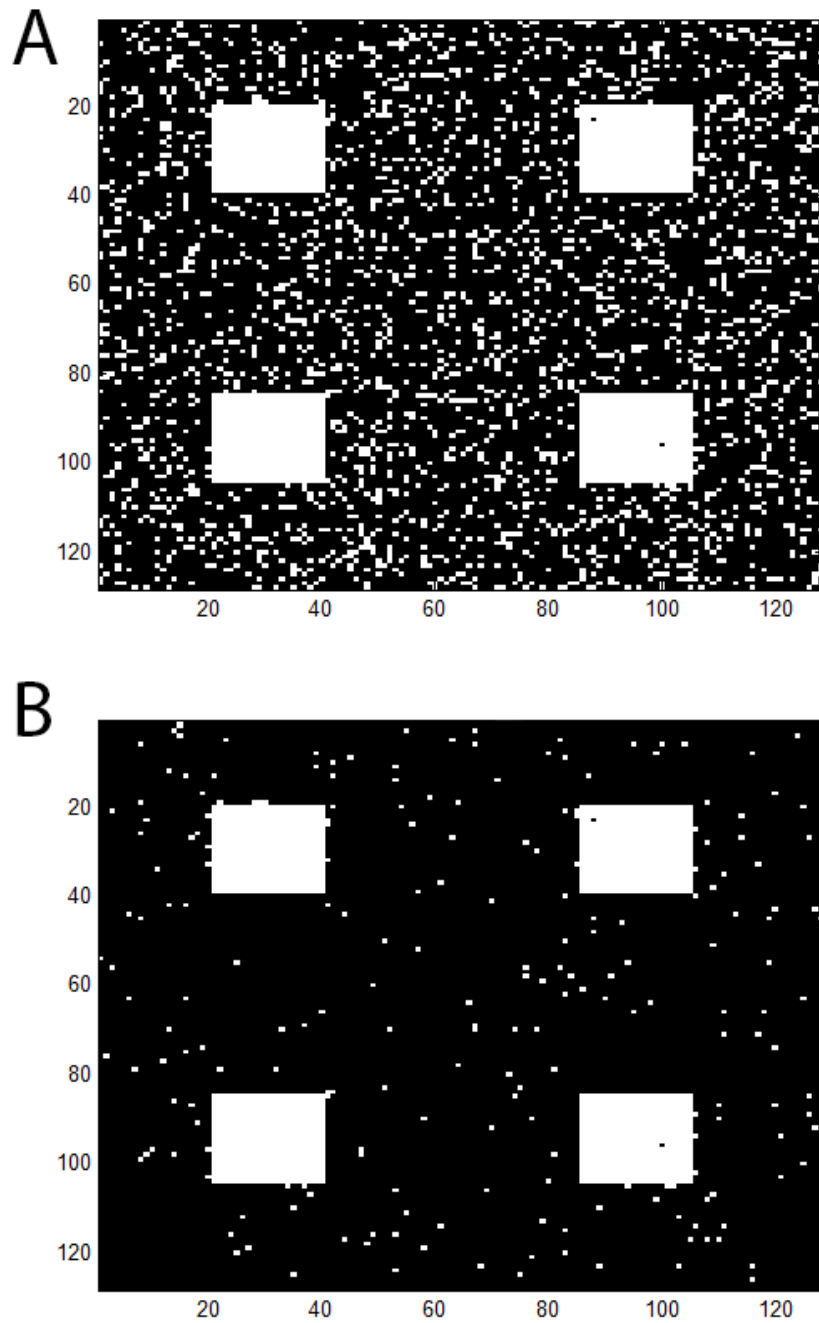
Figure 12: Activation map of CCA and CCA+MSC. A threshold of Z = 1 was applied. CNR of 0.80 was used with kernel size of 0.20. **A:** CCA activation map. **B:** CCA+MSC activation map
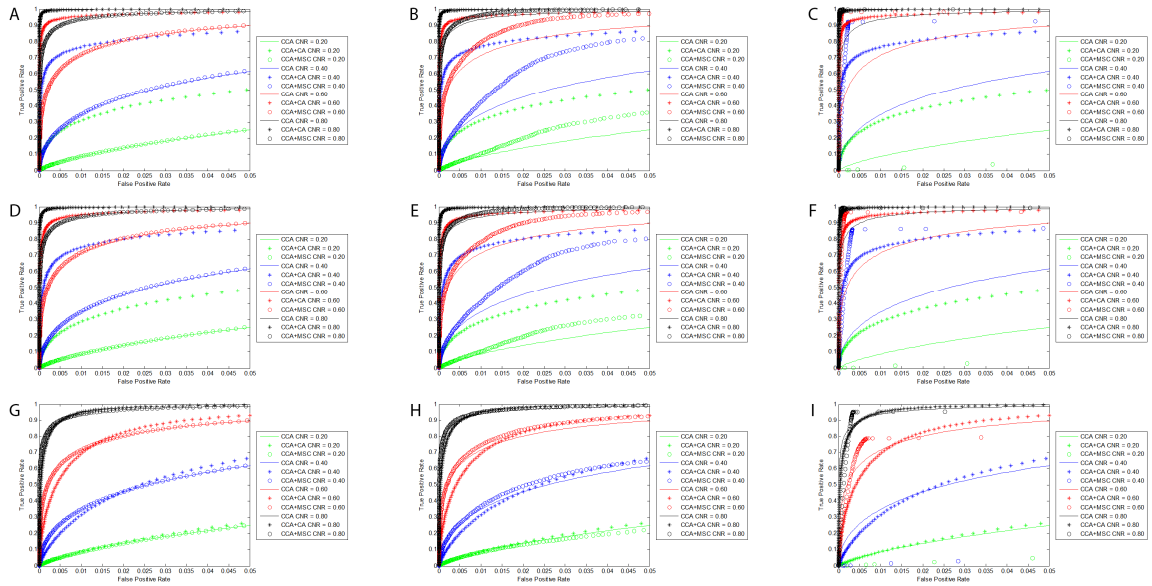
Figure 13: ROC curves for CCA, CCA+CA, CCA+MSC with different kernel sizes and different activation sizes using simulated data. Kernel sizes are 0.10, 0.20, and 0.50. Activation sizes used are 20x20, 10x10, and 2x2. CNRs used are 0.20, 0.40, 0.60, and 0.80. **A:** 20x20 activation size, kernel size = 0.10 **B:** 20x20 activation size, kernel size = 0.20 **C:** 20x20 activation size, kernel size = 0.50 **D:** 10x10 activation size, kernel size = 0.10 **E:** 10x10 activation size, kernel size = 0.20 **F:** 10x10 activation size, kernel size = 0.50 **G:** 2x2 activation size, kernel size = 0.10 **H:** 2x2 activation size, kernel size = 0.20 **I:** 2x2 activation size, kernel size = 0.50
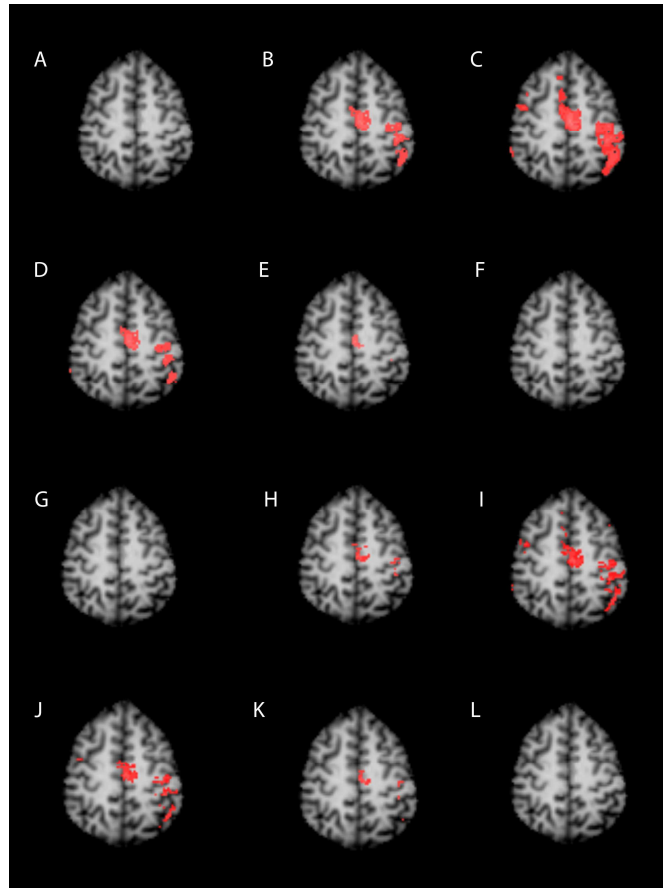
Figure 14: Activation of median nerve stimulation detected with CCA, CCA+CA, CCA+MSC. Significance levels were controlled at p = 0.01 for all images. Z thresholds were changed for each technique based on the significance level. **A:** CCA, Z = 4.8, FWHM = 4mm **B:** CCA+CA, Z = 2.6, cluster size threshold = 6 voxels, FWHM = 4mm **C:** CCA+MSC, Z = 2, kernel size = 0.05, FWHM = 4mm **D:** CCA+MSC, Z = 2, kernel size = 0.10, FWHM = 4mm **E:** CCA+MSC, Z = 2, kernel size = 0.15, FWHM = 4mm **F:** CCA+MSC, Z = 2, kernel size = 0.20, FWHM = 4mm **G:** CCA, Z = 4.8, no filter applied **H:** CCA+CA, Z = 2.6, cluster size threshold = 4 voxels, no filter applied **I:** CCA+MSC, Z = 2, kernel size = 0.05, no filter applied **J:** CCA+MSC, Z = 2, kernel size = 0.10, no filter applied **K:** CCA+MSC, Z = 2, kernel size = 0.15, no filter applied **L:** CCA+MSC, Z = 2, kernel size = 0.20, no filter applied
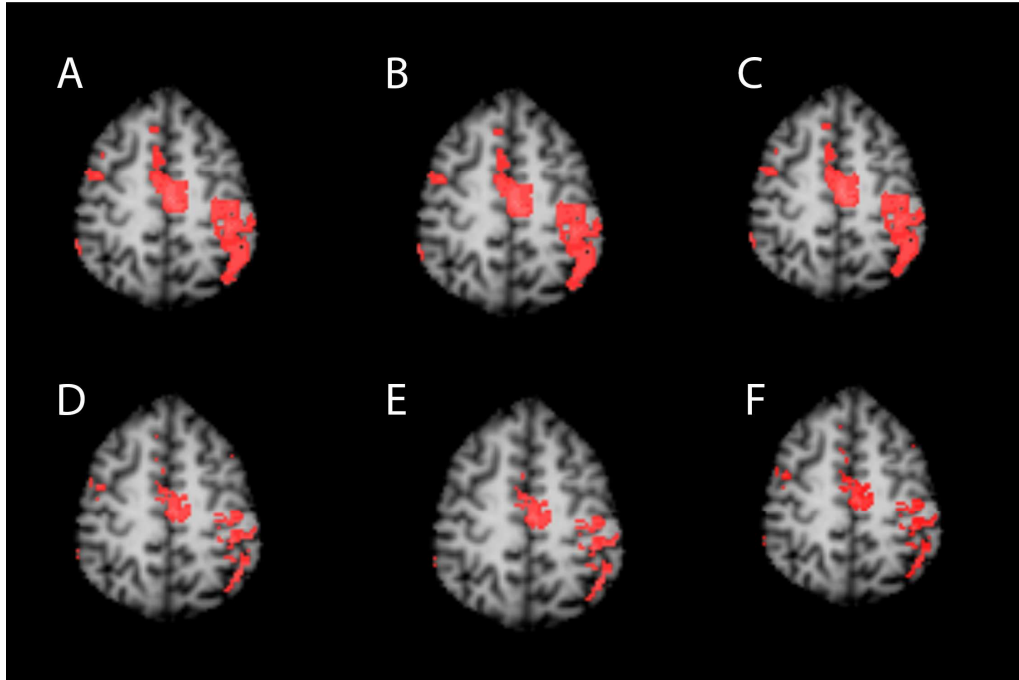
Figure 15: Activation of median nerve stimulation detected with CCA, CCA+CA, CCA+MSC. Z thresholds were controlled at z = 2 for all images. Significance level changes for each technique. **A:** CCA, Z = 2, FWHM = 4mm **B:** CCA+CA, Z = 2, cluster size threshold = 6 voxels, FWHM = 4mm **C:** CCA+MSC, Z = 2, kernel size = 0.05, FWHM = 4mm **D:** CCA, Z = 2, no filter applied **E:** CCA+CA, Z = 2, cluster size threshold = 6 voxels, no filter applied **F:** CCA+MSC, Z = 2, kernel size = 0.05, no filter applied

Table 1: Activation Volume and Average Z-Scores for Averaged Real fMRI Data

	FWHM = 0mm		FWHM = 4mm	
	Volume	Z mean	Volume	Z mean
CCA	0	0.0	0	0.0
CCA+CA	18	3.1	134	3.1
CCA+MSC 0.05	127	2.4	311	2.6
CCA+MSC 0.10	64	2.5	109	3.1
CCA+MSC 0.15	6	3.0	1	4.0
CCA+MSC 0.20	0	0.0	0	0.0

Note: Volumes are measured in voxels.

Table 2: Activation Volume and Average Z-Scores for Individual
Subjects on Real fMRI Data

	FWHM = 0mm						FWHM = 4mm					
	CCA		CCA+CA		CCA+MSC		CCA		CCA+CA		CCA+MSC	
Subject	Volume	Z mean	Volume	Z mean	Volume	Z mean	Volume	Z mean	Volume	Z mean	Volume	Z mean
1	45	7.5	163	5.3	212	6.4	128	7.4	200	6.1	200	6.4
2	20	6.1	114	4.0	169	3.6	18	6.8	106	3.7	181	3.8
3	15	5.8	106	3.9	136	3.5	18	5.8	181	3.6	258	3.2
4	0	0.0	58	3.3	98	2.9	0	0.0	23	3.4	135	2.9
5	102	6.4	251	4.9	265	4.9	182	6.4	390	5.1	395	5.1
6	78	6.6	159	5.2	165	5.1	137	6.7	285	5.2	301	5.1
7	30	6.4	135	4.8	146	4.7	51	6.4	192	4.8	243	5.0
8	0	0.0	41	3.6	60	3.2	6	5.3	64	3.6	88	3.1
9	31	6.3	66	5.0	70	4.9	60	6.3	181	4.6	180	4.5
10	239	8.4	292	7.7	299	7.6	402	9.0	424	8.7	423	8.7
Mean	55.9	5.4	138.5	4.8	162.0	4.7	100.2	6.0	204.6	4.9	240.4	4.8
Standard Deviation	72.0	2.9	81.8	1.2	78.9	1.5	123.1	2.3	130.3	1.6	107.7	1.8

Note: Volumes are measured in voxels.

CHAPTER V

DISCUSSION

Temporal Characteristics Discussion

The results show that the temporal characteristics of msMRI can be detected with both BOLD and msMRI signals seen in overlapping areas of interest (M1). The measured NRF from the time locked averages of the extracted time course does show identifiable temporal characteristics of that is shared with the theoretically calculated NRF, such as the largest peak at roughly 100ms for instance. However, it was also found that the signal could not be reliably detected.

The low sensitivity of msMRI signal detection is likely due to a variety of factors. The NRF used in this study is based on what was reported by Allison et al. (1989). Considering that different subjects were used in this study than Allison et al.'s (1989) study, it is possible that the NRF per subject will not be identical across subjects and that difference is enough to affect the results. Another commonly brought up issue with msMRI signal detection is BOLD contamination. Although a stimulation paradigm designed to minimize BOLD contamination was used, it is still possible that BOLD contamination is masking the msMRI signal in this case as it is unlikely that unwanted BOLD signal has been completely eliminated. Conventional fMRI analysis techniques may also lack the sensitivity to consistently detect the msMRI signal. All of the possible issues are further exacerbated by the fact that the msMRI signal may be very small in reality, possibly as low as 0.2%. As a result, the examination of the msMRI signal's temporal characteristics was temporarily abandoned with the motivation of studying

methods of improving msMRI detection sensitivity from a technique standpoint and from an analysis standpoint.

Despite the issues of detection sensitivity, it is important to investigate the different aspects that contribute to detection sensitivity in msMRI especially since it is known that there are potential problems with currently used fMRI techniques based on cerebral hemodynamics. Temporal resolutions of such techniques are low when compared to neuronal firings because cerebral hemodynamics changes on the order of seconds while neuron activity happens on the order of milliseconds, meaning these techniques cannot detect activity that requires a high temporal resolution. There can also be some concerns about how accurate the detected locations are in actuality as things like drug effects or vasculature of the individual brain can affect regional cerebral hemodynamics. The msMRI technique in principle should address these issues, but the many aspects of detection sensitivity have caused msMRI signal detection to be a matter of debate. Despite this, the aspects of detection sensitivity in msMRI should be investigated not only to strengthen msMRI research, but also because the results from these studies may also improve knowledge on currently used fMRI techniques which may enable better use of the techniques. Although done with the intent to strengthen msMRI research, this work examines two aspects of the detection sensitivity issue (BOLD habituation and MSC) which also can be applied to currently used fMRI techniques and analysis.

Habituation Discussion

Using median nerve stimulation and BOLD fMRI, the hemodynamic habituation effect was observed in the experiment. The data shows that the habituation effect is quite severe between runs as only the first run showed a detectable activation on average. The data also shows that significant decay happens within the duration of the first scan that was performed in the series of seven. It would not be unreasonable to conclude that there is a strong habituation effect with cerebral hemodynamics associated with median nerve stimulation.

The habituation of cerebral hemodynamics found in our data are consistent with other types of stimulations such as visual, auditory, motor, and pain (Becerra et al. 1999, Dirnberger et al. 2004, Fischer et al. 2000, Pfeiderer et al. 2002, Mosbascher et al. 2010, Seitz et al. 1992, Talavage et al. 1999, Taylor et al. 1978, Tomberg et al. 1989). Most of these studies were designed to study the habituation effect, and they have reported decreases in signal in their findings after repeated stimulations over time. While the stimulation type varied across studies, hemodynamic habituation is a common finding. Our study using repeated median nerve stimulation over time also found hemodynamic habituation, which is consistent with the aforementioned studies.

Several other groups have studied median nerve stimulation using fMRI (Arthurs et al. 2004, Backes et al. 2000, Ferretti et al. 2003, Feretti et al. 2007). However, these studies were designed to investigate attention effects and other effects. They did not have a focus on hemodynamic habituation effects. Subjects performed different tasks during the studies and/or received magnitude varying-stimuli, which could potentially mask habituation. Results from such studies would likely be dominated by the main task effects

of the different stimulation paradigms. None of these studies have specifically mentioned any habituation effect. Even if it were to be assumed that the habituation effects were not masked, none of these studies showed a change in recorded BOLD signal as severe as is seen in the presented results. The presented study used an identically repeated stimulation with the volunteer passively feeling the stimulation. Severe habituation in the BOLD signal was observed. This would suggest that non identically repeated stimuli and tasks do in fact mask or minimize habituation effects or cause enough differences that habituation does not occur. It may also be worth noting that it is not unreasonable to consider the possibility that the subjects' attention to the stimuli could be in different states for the duration of the scan, thus the attention effect cannot be completely discounted as a contributor to the severe signal decrease seen in the presented data.

Since the BOLD signal is coupled to evoked potentials, measuring BOLD signal and neuronal activity concurrently offers an opportunity to study the coupling relationship. Janz et al. (2001) examined this relationship using BOLD fMRI and Visual Evoked Potentials (VEP). Their fMRI results show a maximum signal change of 1.2 - 2.9% after approximately ten seconds. Their VEP results show a curve with a continuous decline that they state can be described with an exponential with a time constant of 14.7 ± 2.1 seconds. When comparing the VEP and BOLD signals, their conclusion states that the BOLD signal time course was not being accurately predicted with a linear model. The coupling between evoked potentials and hemodynamic response would appear to be rather complex, though Janz et al. (2001) themselves do not offer any particular insight into this relationship beyond what was already stated.

Unlike hemodynamic response which shows significant habituation across a wide range of stimuli, evoked potentials of the MNS over repeated stimulations is apparently not as simple. It has been reported that the overall signal strength of evoked potentials in the brain does not vary significantly over repeated median nerve stimulation, suggesting that habituation effects are not significant (Thees et al. 2003). However there are also studies that have shown that specific peaks in the waveform (e.g., N20) are susceptible to severe habituation (Ozkul et al. 2002, Restuccia et al. 2011). This raises the question of how the cerebral hemodynamics is coupled with neuronal activity. One possible explanation is that cerebral hemodynamics is coupled to the overall signal strength of evoked potentials. If this is true, then the coupling relationship between cerebral hemodynamics and evoked potentials must decrease over repeated stimulations. Only if the coupling relationship decreases over time can it possibly explain the relationship of a constant evoked potentials and a decreased hemodynamic response for the repeated MNS as seen in the presented results. Another possible explanation is the cerebral hemodynamics are coupled to specific peaks of evoked potentials (e.g., N20) instead of the overall signal strength. As it is known that specific peaks can be susceptible to severe habituation, coupling cerebral hemodynamics with specific peaks would likely show a decrease in the detected activation if habituation were to occur, explaining the habituation observed in our results. It should be noted that comparable evoked potential data (e.g., same subjects, same stimuli, etc.) was not collected for the purpose of this study. As a result, this study is not able to differentiate which possible explanations for the phenomenon are more likely, or if there are other explanations (such as attention effects). Further investigations of the coupling between evoked potentials and cerebral

hemodynamics as well as the behavior of coupling over repeated stimulations would be needed.

In summary, we have found severe habituation in BOLD signals when using median nerve stimulation. Between the seven runs performed, the habituation can be seen very quickly as activations were detected only in the first run on average. Within the first run, statistically significant BOLD signal decay was identified when using split-half analysis. The observed habituation is consistent with other studies that have focused on hemodynamic habituation using various types of stimulation. However, the results are not consistent with studies that have focused on evoked potentials with median nerve stimulation. The results do raise the question of how evoked potentials relates to cerebral hemodynamics when examined over a period of time with the presented scenario. It is possible that the coupling relationship between cerebral hemodynamics and evoked potentials decreases over time. Another possibility is that cerebral hemodynamics and evoked potentials are coupled with specific peaks within the electric waveform that are susceptible to severe habituation. As no evoked potential data was collected for this study, we are not able to determine which of these scenarios are more likely, or if there are other explanations for the phenomenon. Further investigations would be required to determine the underlying cause of the hemodynamic habituation seen in our results.

MSC Discussion

In this study, the adoption of MSC into fMRI analysis was examined by comparing it to CCA and CCA+CA. The ROC curves (Figure 13) indicate that the proposed MSC technique show an improvement over CCA and can show improvements

over or similar results when compared to CCA+CA. The false positive rate comparisons (Figure 11) showed significant improvement over CCA which indicates that CCA+MSC controls noise very well. This allows a lower statistical threshold to be used when identifying activations (Figure 12). Another potential benefit of MSC is for highly focused activation detection since no cluster threshold is applied.

The performance of CCA+MSC depends on the kernel size being used (Figure 10), but determining an optimal range of kernel sizes is not a trivial issue. If the kernel size used is too large, potentially no activations would be detected. Conversely, if the kernel size used is too small, the proposed technique does not show an improvement when compared to CCA and CCA+CA. A proper kernel size needs to be used in order to see an improvement over CCA and CCA+CA. When tested with simulated data, the ROC curves and true positive comparison indicate that a kernel size of roughly 0.20 is a reasonable kernel size to use and should show an improvement over CCA (Figures 10 and 13), but no activations were detected with real fMRI data at that kernel size. Real fMRI data showed activations at kernel size of 0.05 and 0.10 (Figure 14). The difference in optimal kernel sizes between the real and simulated data may be explained by the different noise characteristics of the data. The simulated data is the ideal situation with only Gaussian white noise. Real fMRI data has multiple noise types such as movement artifacts, physiological noise, noise from the MRI machine itself, etc. It is likely that the optimal kernel size depends on the structure of noise in the data and needs optimized for each individual data set. Future studies are required to examine this issue in more detail.

Significant improvement is seen with CCA+MSC over CCA on the simulated data in the ROC curves at a kernel size of 0.50 at CNRs 0.40 (not 2x2 case), 0.60, and

0.80 (Figures 13C, F and I), but this improvement is sudden and is concentrated in the region of false positive rates up to 0.05. While this type of improvement is typically unexpected, it is mostly consistent with Figure 10 where larger kernel sizes does result in detection of true positives, but Figures 10 and 13 are not necessarily directly comparable. Also, kernel size 0.50 was not included in all comparisons for this study because Figure 10 does not show it to be useful at all CNRs.

The false positive rate comparison for the 2x2 test pattern showed a curve that is more similar to the CCA curve than the 10x10 and 20x20 cases (Figure 11). This may be due to the 2x2 case having many more neighboring voxels adjacent the test pattern than the other cases. Four 20x20 test patterns were inserted into simulated fMRI images, which results in 320 neighboring voxels. To maintain the same total area of the test pattern, four hundred 2x2 activations were used, resulting in 3200 neighboring voxels. The 2x2 test image has ten times the number of voxels that are directly adjacent the inserted activations when compared to the 20x20 test image. It is more likely for falsely activated voxels to be detected by cluster analysis techniques if it is attached to the test pattern than when isolated. More falsely activated voxels are expected to be detected for the 2x2 test pattern, thus increasing the false positive rate. Regardless, the proposed technique still shows improvement when compared to CCA in the 2x2 case.

CCA+MSC can show similar results when compared to CCA+CA at a false positive rate of greater than about 0.04 with a kernel size of 0.20 (Figure 13), but this similarity is not seen in the 2x2 case where CCA+MSC was either slightly improved or about the same as CCA+CA. A cluster threshold of 4 voxels was used to set the significance value at $p = 0.01$, which also happens to be the exact size of the simulated

activations in the 2x2 case. If the activation size was three voxels or a different significance level was used and the voxel cluster threshold was increased, the activations would have been removed by the cluster analysis. The CCA+MSC technique by itself does not have a cluster threshold and has the potential of better detecting highly focused activations.

The selection of image characteristics used in the feature space should be examined in future studies as the feature space likely has a large effect on the results as well as the range of acceptable kernel sizes. The image characteristics selected for the featured space used in this study was the estimated Z values found in the SPI and the mean voxel values surrounding a voxel in the SPI. While there are many methods of constructing a feature space, the feature space used did show an improvement over CCA in the simulated and real fMRI data at the same significance level, it is unknown what image features or what combination of image feature produces the best feature space for fMRI analysis. The feature space used in this study does not incorporate temporal features in the data or positional features for example. There may be other types and combinations of image features that can be used, and it would certainly be an area of further examination.

The proposed technique has the limitation that the significance levels cannot be easily theoretically calculated (or at least a method has yet to be implemented at the time of this writing). This presents a particular drawback when doing comparisons. Significance levels can be approximated using simulations as was done in this study, but still may present some challenges when very accurate comparisons are required.

The experiment performed in this study examines the application of MSC to CCA in fMRI activation detection. The results show that an improvement with CCA+MSC can be seen over the typical CCA and CCA+CA analysis technique. The proposed technique maintains a lower false positive rate than CCA which allows the use of lower statistical thresholds while controlling for noise and helps activation detection in low CNR situations. This also helps in detecting small highly focused activations especially considering that CCA+MSC does not require the application of a cluster size threshold, which is required by most cluster analysis techniques. By nature, CCA+MSC also has the ability to incorporate different image characteristics into a feature space for analysis. These benefits can help to improve activation detection in fMRI data. However, studies in the optimization in kernel size and feature space are needed to further develop the proposed technique. Despite the aforementioned limitations, the proposed technique shows promise in improving fMRI activation detection.

Discussion With Relation to msMRI

The results from the experiments performed show that it is possible to further address some of the concerns that have caused msMRI signal detection to be a matter of debate. The habituation study performed shows that the BOLD signal decays rapidly with repeated median nerve stimulation, which gives insight on when BOLD contamination is more likely to be an issue within the context of msMRI signal detection. The adoption of MSC into fMRI analysis showed that the proposed MSC technique can show improvements over currently used fMRI analysis techniques, which may have applications in msMRI to address the issue of its signal being very small.

The habituation study showed that the BOLD effects due to identically repeated electrical median nerve stimulation become rapidly undetectable on average, indicating that cases exist where BOLD contamination may be less of an issue in the context of msMRI research. In such a scenario, if an msMRI signal is detected, it would be less likely for it to be noise caused by BOLD contamination, giving more strength to research on msMRI signal detection. While this could strengthen msMRI research, it requires further examination to fully understand the phenomenon as there are other issues that can affect regional cerebral hemodynamics thus affecting how much BOLD contamination may be present. For example, attention effects have been shown to have an effect on the detected BOLD signal, which may in turn have an effect on msMRI signal detection. Although the results of this experiment show the BOLD signal being undetectable after a certain amount of time, the BOLD signal in actuality does not truly vanish. If any BOLD signals do not meet the criteria set by the analysis method, the BOLD signal has simply been defined as not present, but can still have an effect on the msMRI signals especially considering that previous experimental data has shown how small the msMRI signal can be in actuality. More examinations are needed to fully understand these issues.

The application of MSC into fMRI analysis shows that there are a variety of benefits that may be applied to msMRI analysis. The results show that incorporating MSC into fMRI analysis controls false positive rates well compared to the commonly used CCA analysis even in low CNR situations, allowing the use of lower statistical thresholds compared to CCA. Considering that one of the issues surrounding msMRI signal detection is that the signal itself may be very small according to experimental data, the applying of MSC to the msMRI analysis could help to alleviate some of these

concerns. MSC can also show benefits when detecting highly focused activations compared to CCA and CCA+CA if properly optimized as msMRI activations can be considered to be highly focused, thus it would be less likely to be removed by the aforementioned cluster thresholds while retaining the other benefits of the MSC technique. However, what was done for the purposes of this study may not be ideal for use in msMRI research or fMRI research in general. The feature space used for this study, while not arbitrarily selected, may not be optimal for msMRI research or for fMRI analysis. Further examinations in feature spaces, among other needed optimizations such as kernel sizes, would need to be performed before this technique can be realistically applied in a practical setting.

Summary

In summary, this work examines the feasibility of msMRI by studying possible acquisition strategies and data analysis strategies. Detection of the temporal characteristics of the msMRI signal is possible, where the largest peak at about 100ms can be detected. However, the inconsistent detection of the temporal characteristics motivated the aforementioned studies. BOLD habituation was examined to identify under what conditions the BOLD signal would be reduced. MSC was applied to fMRI analysis to examine if detection sensitivity can be improved.

The BOLD habituation study showed the BOLD signal habituating severely, to the point of being undetectable within the first MRI run, using identically repeated median nerve stimulation. By understanding what causes this situation and being able to replicate it reliably, it would be possible to reduce the issue of BOLD contamination in

the context of msMRI signal detection. Targeting when the BOLD signal has habituated away for msMRI signal detection should reduce the issue of BOLD contamination as the BOLD signal itself is undetectable or at a minimum.

Applying MSC to fMRI analysis improves the analysis results when compared to the commonly used CCA and CCA+CA in certain situations. MSC controls false positive rates well compared to CCA and CCA+CA in low CNR situations and can improve detection of highly focused activations if properly optimized. Since the msMRI signal can be very small in magnitude and highly focused, the MSC technique can help to identify msMRI activations if optimization is achieved. The feature space used in this study is similar to other cluster analysis techniques in concept (magnitude and neighbors), and incorporating other features, temporal features for example, can further the examination of MSC in msMRI and fMRI analysis.

BIBLIOGRAPHY

Allison T, McCarthy G, Wood CC, Darcey TM, Spender DD, Williamson PD. Human cortical potentials evoked by stimulation of the median nerve. I. Cytoarchitectonic areas generating short-latency activity. J Neurophysiol 1989a; 62:694-710

Allison T, McCarthy G, Wood CC, Williamson PD, Spender DD. Human Cortical Potentials Evoked by Stimulation of the Median Nerve. II. Cytoarchitectonic Areas Generating Long-Latency Activity. J Neurophysiol 1989b; 62:711-722

Arthurs OJ, Johansen-Berg H, Matthews PM, Boniface SJ. Attention differentially modulates the coupling of fMRI BOLD and evoked potential signal amplitudes in the human somatosensory cortex. Exp Brain Res 2004; 157:269–274

Backes WH, Mess WH, Kranen-Mastenbroek V, Reulen JP. Somatosensory cortex responses to median nerve stimulation: fMRI effects of current amplitude and selective attention. Clin Neurophysiol 2000; 111:1738-1744

Bandettini, P.A. 1992. Time course EPI of human brain function during task activation. Magn. Reson. Med. 25, 390-397.

Bandettini P, Jesmanowicz A, Wong E, Hyde J: Processing strategies for time-course data sets in functional MRI of the human brain. Magn Reson Med 1993, 30(2), 161-173

Baumgartner R, Scarth G, Teichtmeister C, Somorjai R, Moser E: Fuzzy Clustering of Gradient-Echo Functional MRI in the Human Visual Cortex Part I: Reproducibility. J. Magn Reson Imag 1997, 7(6), 1094-1101

Baumgartner R, Windischberger C, Moser E: Quantification in Functional Magnetic Resonance Imaging: Fuzzy Clustering vs Correlation Analysis. Magn Reson Imag 1998, 16(2), 115-125

Becerra LR, Breiter HC, Stojanovic M, Fishman S, Edwards A, Comite A, Gonzalez R, Borsook D (1999). Human brain activation under controlled thermal stimulation and habituation to noxious heat: an fMRI study. Magn Reson Med 1999; 41:1044–1057

Belliveau, J.W. 1991. Functional mapping of the human visual cortex by magnetic resonance imaging. Science 254, 716-719.

Bezdek J, Ehrlich R, Full W, 1984. FCM: The fuzzy C-Means Clustering Algorithm. Comput Geosci, 10(2), 191-203

Bianciardi M. 2004. Combination of BOLD-fMRI and VEP recordings for spin-echo MRI detection of primary magnetic effects caused by neuronal currents. Magn Reson Imaging 22: 1429-1440.

Blagoev, K.B. 2007. Modelling the magnetic signature of neuronal tissue. NeuroImage 37: 137-148.

Bodurka, J. 2002. Toward direct mapping of neuronal activity: MRI detection of ultraweak, transient magnetic field changes. Magn Reson Med 47: 1052-1058.

Bodurka, J. 1999. Current-induced magnetic resonance phase imaging. J Magn Reson 137: 265-271.

Boynton G, Engel S, Glover G, Heeger D: Linear systems analysis of functional magnetic resonance imaging in human. J Neurosci 1996, 16(13), 4207-4221

Bullmore E, Brammer M, Williams SCR, Rabe-Hesketh S, Janot N, David A, Mellers J, Howard R, Sham P: Statistical methods of estimation and inference for functional MR image analysis. Magn Reson Med 1996, 35(2), 261–277

Cassara, A.M. 2008. Realistic simulations of neuronal activity: A contribution to the debate on direct detection of neuronal currents by MRI. NeuroImage 39:87-106.

Calhoun V, Adali T, McGinty V, Pekar J, Watson T, Pearlson G: fMRI Activation in a Visual-Perception Task: Network of Areas Detected Using the General Linear Model and Independent Components Analysis. NeuroImage 2001, 14(5), 1080-1088

Cheng Y: Mean shift, Mode seeking, and Clustering. IEEE Trans Pattern Anal Mach Intell 1995, 17(8), 790-799

Chow, L.S. 2006a. Investigating direct detection of axon firing in the adult human optic nerve using MRI. Neuroimage 30: 835-846.

Chow, L.S. 2006b. Investigation of MR signal modulation due to magnetic fields from neuronal currents in the adult human optic nerve and visual cortex. Magn Reson Imaging 24: 681-691.

Cohen, D., 1968. Magnetoencephalography: evidence of magnetic fields produced by alpha-rhythm currents. Science 161: 784-786.

Cohen M: Parametric Analysis of fMRI Data Using Linear Systems Methods. NeuroImage 1997, 6(2), 93-103

Connolly C: The relationship between colour metrics and the appearance of three-dimensional coloured objects. Color Res Appl 1996, 21:331-337

Cox R: AFNI: Software for Analysis and Visualition of Functional Magnetic Resonance Neuroimages. Comput Biomed Res 1996, 29(3), 169-173

Dirnberger G, Duregger C, Lindinger G, Lang W. Habituation in a simple repetitive motor task: a study with movement-related cortical potentials. Clin Neurophysiol 2004; 115:379-384

Dorin C, Peter M: Mean Shift: A Robust approach towards feature space analysis. IEEE Trans Pattern Anal Mach Intell 2002, 24(5), 603-619

Ferretti A, Babiloni C, Gratta C, Caulo M, Tartaro A, Bonomo L, Rossini PM, Romani GL. Functional topography of the secondary somatosensory cortex for nonpainful and painful stimuli: an fMRI study. NeuroImage 2003; 20:1625-1638

Ferretti A, Babiloni C, Arienzo D, Gratta C, Rossini RM, Tartaro A, Romani GL. Cortical Brain Responses during Passive Nonpainful Median Nerve Stimulation at Low Frequencies (0.5–4 Hz): An fMRI Study. Hum Brain Mapp 2007; 28:645-653

Fischer H, Furmark T, Wik G, Fredrikson M. Brain representation of habituation to repeated complex visual stimulation studied with PET. NeuroReport 2000; 11:123-126

Foreman S, Cohen J, Fitzgerald M, Eddy W, Mintun M, Noll D: Improved Assessment of Significant Activation in Functional Magnetic Resonance Imaging (fMRI): Use of a Cluster-Size Threshold. Magn Res Med 1995, 33(5), 636-647

Fox PT, Raichle ME (1986). Focal physiological uncoupling of cerebral blood flow and oxidative metabolism during somatosensory stimulation in human subjects. Proc. Natl. Acad. Sci. USA. 83(4):1140-4.

Friston K, Holmes A, Worsley K, Poline J, Frith C, Frackowaik R: Statistical Parametric Maps in Functional Imaging: A General Linear Approach. Hum Brain Mapp 2004, 2(4), 189-210

Fukunaga K, Hostetler L: The Estimation of the Gradient of a Density Function, with Applications in Pattern Recognition. IEEE Trans Inf Theory 1975, 21(1), 32-40

Heeger DJ, Huk AC, Geisler WS, Albrecht DG. Spikes versus BOLD: what does neuroimaging tell us about neuronal activity?. Nat Neurosci 2000; 3:631–633

Janz C, Heinrich SP, Kornmayer J, Bach M, Hennig J. Coupling of Neural Activity and BOLD fMRI Response: New Insights by Combination of fMRI and VEP Experiments in Transition From Single Events to Continuous Stimulation. Magn Reson Med 2001; 46:482-486

Konn, D. 2003. MRI detection of weak magnetic fields due to an extended current dipole in a conducting sphere: a model for direct detection of neuronal currents in the brain. Magn Reson Med 50: 40-49.

Kwong K, Belliveau J, Chesler D, Goldberg I, Weisskoff R, Poncelet B, Kennedy D, Hoppel B, Cohen M, Turner R, Cheng HM, Brady T, Rosen B. Dynamic magnetic resonance imaging of human brain activity during primary sensory stimulation. Pro Natl Acad Sci USA 1992; 89:5675-5679

Lai S (1993). Identification of vascular structures as a major source of signal contrast in high resolution 2D and 3D functional activation imaging of the motor cortex at 1.5T: preliminary results. Magn Reson Med. 30:387-392

Liston, A.D. 2004. The MR detection of neuronal depolarization during 3-Hz spike-and-wave complexes in generalized epilepsy. Magn Reson Imaging 22: 1441-1444.

Logothetis NK, Pauls J, Augath M, Trinath T, Oeltermann A. Neurophysiological investigation of the basis of the fMRI signal. Nature 2001; 412:150–157

MacQueen J: Some Methods for Classification and Analysis of Multivariate Observatoins. Proceedings of 5th Berkeley Symposium on Mathematical Statistics and Probability, University of California Press 1967, pp. 281-297

Mayer A, Greenspan H: An Adaptive Mean-Shift Framework for MRI Brain Segmentation. IEEE Trans Med Imag 2009, 28(8), 1238-1250

Mosbascher A, Brinkmeyer J, Warbrick T, Musso F, Schlemper V, Wittsack HJ, Saleh A, Schnitzler A, Winterer G. Brain activation patterns underlying fast habituation to painful laser stimuli. Int J Psychophysiol 2010; 75:16-24

Moser E, Diemling M, Baumgartner R: Fuzzy clustering of gradient-echo functional MRI in the human visual cortex. Part II: Quantification. J. Magn Reson Imag 1997, 7(6), 1102–1108

Ogawa S, Lee TM, Kay AR, Tank DW. Brain magnetic resonance imaging with contrast dependent on blood oxygenation. Proc Natl Acad Sci USA 1990; 87:9868 –9872.

Ozkul Y, Uckardes A. Median nerve somatosensory evoked potentials in migraine. Eur J Neurol 2002; 9:227–232

Pfeiderer B, Ostermann J, Michael N, Heindel W. Visualization of Auditory Habituation by fMRI. NeuroImage 2002; 17:1705-1710

Pell, G.S. 2006. Further steps toward direct magnetic resonance (MR) imaging detection of neural action currents: Optimization of MR sensitivity to transient and weak currents in a conductor. Magn Reson Med 55: 1038-1046.

Penny W, Friston K: Mixtures of general linear models for functional neuroimaging. IEEE Trans Med Imag 2003, 22(4), 504-514

Petridou, N. 2006. Direct magnetic resonance detection of neuronal electrical activity. Proc Natl Acad Sci USA 103: 16015-16020.

Restuccia D, Piero ID, Martucci L, Zanini S. High-frequency oscillations after median-nerve stimulation do not undergo habituation: A new insight on their functional meaning?. Clin Neurophysiol 2011; 122:148–152

Schulz, M., Chau, W., Graham, S.J., McIntosh, A.R., Ross, B., Ishii, R., Pantev, C., (2004). An integrative MEG-fMRI study of the primary somatosensory cortex using cross-modal correspondence analysis. NeuroImage 22, 120-133.

Scott, G.C, 1992. RF current density imaging in homogeneous media. Magn Reson Med 28: 186-201.

Seitz RJ, Roland PE. Learning of Sequential Finger Movements in Man: a Combined Kinematic and Positron emission Tomography (PET) Study. Eur J Neurosci 1992; 4:154-165

Singh M, Patel P, Khosla D, Kim T: Segmentation of functional MRI by K-Means Clustering. IEEE Trans Nucl Sci 1996, 43(3), 2030-2036

Song, A.W. 2001. Lorentz effect imaging. Magn Reson Imaging 19: 763-767.

Swinney K, Wikswo J (1980). A calculation of the magnetic field of a nerve action potential. Biophys. J. 32(2):719-31.

Talavage TM, Edminster WB, Ledden PJ, Weisskoff RM. Quantitative Assessment of Auditory Cortex Responses Induced by Imager Acoustic Noise. Hum Brain Mapp 1999; 7:79-88

Thees S, Blankenburg F, Taskin B, Curio G, Villringer A. Dipole source localization and fMRI of simultaneously recorded data applied to somatosensory categorization. NeuroImage 2003; 18:707-719

Tomberg C, Desmedt KE, Ozaki I, Nguyen TH, Chalklin V. Mapping somatosensory evoked potentials to finger stimulation at intervals of 450 to 4000 msec and the issue of habituation when assessing early cognitive components. Electroencephalogr Clin Neurophysiol 1989; 74:347-358

Taylor MJ. Bereitschaftspotential During the Acquisition of a Skilled Motor Task. Electroencephalogr Clin Neurophysiol 1978; 45:568-576

Truong, T.K. 2006. Finding neuroelectric activity under magnetic-field oscillations (NAMO) with magnetic resonance imaging in vivo. Proc Natl Acad Sci USA 103: 12598-12601.

Worsley K, Evans A, Marrett, S, Neelin P: Three-dimensional statistical analysis for CBF activation studies in human brain. J Cereb Blood Flow Metab 1992, 12(6), 900 – 918

Wyszecki G, Stilles W: Color Science: Concepts and Methods, Quantitative Data, and Formulae. J Wiley, New York; 1982

Xiong J, Gao J, Lancaster J, Fox P: Clustered Pixel Analysis for Functional MRI Activation Studies of the Human Brain. Hum Brain Mapp 1995, 4(4), 287-301

Xiong, J. 2003. Directly mapping magnetic field effects of neuronal activity by magnetic resonance imaging. Human Brain Mapp 20, 41-49.

Xue Y, Gao JH, Xiong J (2006). Direct MRI Detection of Neuronal Magnetic Fields in the Brain: Theoretical Modeling. NeuroImage 31(2):550-559.

Xue Y, Chen X, Grabowski T, Xiong J (2009). Direct MRI Mapping of Neuronal Activity Evoked by Electrical Stimulation of the Median Nerve at the Right Wrist. Magn Reson Med